bioRxiv preprint doi: https://doi.org/10.1101/2021.07.30.454416; this version posted October 15, 2021. The copyright holder for this preprint (which was not certified by peer review) is the author/funder, who has granted bioRxiv a license to display the preprint in perpetuity. It is made available under aCC-BY-NC 4.0 International license.

AtpΘ is an inhibitor of F_0F_1 ATP synthase to arrest ATP hydrolysis during low-energy conditions in cyanobacteria

Kuo Song[1], Desirée Baumgartner[1,§], Martin Hagemann[2], Alicia M. Muro-Pastor[3], Sandra Maaß[4], Dörte Becher[4],and Wolfgang R. Hess[1,*]

[1]University of Freiburg, Faculty of Biology, Genetics and Experimental Bioinformatics, Schänzlestr. 1, D-79104 Freiburg, Germany;

[2]University of Rostock, Institute of Biosciences, Plant Physiology Department, Albert-Einstein-Str. 3, D-18059 Rostock, Germany;

[3]Instituto de Bioquímica Vegetal y Fotosíntesis, Consejo Superior de Investigaciones Científicas and Universidad de Sevilla, E-41092 Sevilla, Spain;

[4]University of Greifswald, Department of Microbial Proteomics, Institute of Microbiology, D-17489 Greifswald, Germany.

***Lead contact:** wolfgang.hess@biologie.uni-freiburg.de, University of Freiburg, Faculty of Biology, Genetics and Experimental Bioinformatics, Schänzlestr. 1, D-79104 Freiburg, Germany; phone: +49-761-2032796; FAX: +49-761-2032745.

[§]Current address: Laboratory for MEMS Applications, IMTEK - Department of Microsystems Engineering, University of Freiburg, Georges-Köhler-Allee 103, D-79110 Freiburg, Germany

bioRxiv preprint doi: https://doi.org/10.1101/2021.07.30.454416; this version posted October 15, 2021. The copyright holder for this preprint (which was not certified by peer review) is the author/funder, who has granted bioRxiv a license to display the preprint in perpetuity. It is made available under aCC-BY-NC 4.0 International license.

Summary

Biological processes in all living cells are powered by ATP, a nearly universal molecule of energy transfer. ATP synthases produce ATP utilizing proton gradients that are usually generated by either respiration or photosynthesis. However, cyanobacteria are unique in combining photosynthetic and respiratory electron transport chains in the same membrane system, the thylakoids. How cyanobacteria prevent the futile reverse operation of ATP synthase under unfavorable conditions pumping protons while hydrolyzing ATP is mostly unclear. Here, we provide evidence that the small protein AtpΘ, which is widely conserved in cyanobacteria, is mainly fulfilling this task. The expression of AtpΘ becomes induced under conditions such as darkness or heat shock, which can lead to a weakening of the proton gradient. Translational fusions of AtpΘ to the green fluorescent protein revealed targeting to the thylakoid membrane. Immunoprecipitation assays followed by mass spectrometry and far Western blots identified subunits of ATP synthase as interacting partners of AtpΘ. ATP hydrolysis assays with isolated membrane fractions as well as purified ATP synthase complexes demonstrated that AtpΘ inhibits ATPase activity in a dose-dependent manner similar to the F_0F_1-ATP synthase inhibitor N,N-dicyclohexylcarbodimide. The results show that, even in a well-investigated process, crucial new players can be discovered if small proteins are taken into consideration and indicate that ATP synthase activity can be controlled in surprisingly different ways.

Keywords: ATP synthase, cyanobacteria, *Synechocystis*, small proteins

bioRxiv preprint doi: https://doi.org/10.1101/2021.07.30.454416; this version posted October 15, 2021. The copyright holder for this preprint (which was not certified by peer review) is the author/funder, who has granted bioRxiv a license to display the preprint in perpetuity. It is made available under aCC-BY-NC 4.0 International license.

Introduction

ATP synthases of the F_0F_1 type are multisubunit protein complexes anchored to membranes that convert proton (or sodium ion) gradients into chemical energy in the form of ATP[1]. Proton gradients are established by divergent processes, such as respiratory electron transport in mitochondria or photosynthetic electron transport in chloroplasts. Mitochondria and chloroplasts originate from the endosymbiotic uptake of an α-proteobacterium and a cyanobacterium, respectively[2–7]. Therefore, it is not surprising that F_0F_1-ATP synthases share close functional and structural similarities among eukaryotes and bacteria.

Under conditions weakening the proton gradient, ATP synthases can operate backwards, pumping protons while hydrolyzing ATP. Therefore, different regulatory mechanisms have evolved to stop the futile reverse reaction. Mitochondrial ATP synthases employ small peptides for inhibition, one, designated inhibitory factor 1 (IF1), in mammals[8,9] and three, called IF1, STF1 and STF2, in yeast[10,11]. IF1 inhibits the ATPase activity of mitochondrial ATP synthase under conditions when the membrane potential collapses, e.g., during anoxia in cancer cells[12]. In bacteria, some regulatory factors of ATP synthase are known as well, such as the ζ subunit in *Paracoccus denitrificans* and related α-proteobacteria[13], but IF1, as a representative of the class of alpha-helical basic peptide inhibitors in eukaryotes, has no homologs among prokaryotes.

Plant chloroplasts, in contrast, use a different mechanism to inhibit the hydrolysis activity of ATP synthase. Here, the γ subunit encoded by *atpC* responds to redox signals, thereby preventing the back reaction of ATP synthase when the photosynthetic proton gradient ceases, particularly during the night[14]. The *atpC* gene and the encoded γ subunit in chloroplasts are very similar to their homologs from

bioRxiv preprint doi: https://doi.org/10.1101/2021.07.30.454416; this version posted October 15, 2021. The copyright holder for this preprint (which was not certified by peer review) is the author/funder, who has granted bioRxiv a license to display the preprint in perpetuity. It is made available under aCC-BY-NC 4.0 International license.

cyanobacteria, consistent with the endosymbiotic origin of chloroplast ATP synthase from an ancient cyanobacterium[15]. The chloroplast γ subunit, however, possesses a short insertion of nine extra amino acids (–EICDINGXC–), including two cysteine residues[16] that can form a disulfide bond under oxidizing conditions, which entirely blocks rotation and prevents ATP hydrolysis[1]. Upon illumination, the chloroplasts become reduced, and the disulfide bridge in the γ subunit opens, which activates ATP synthase because the γ subunit can rotate freely. The respective nine-amino-acid insertion in chloroplast γ subunits is strictly conserved in plants but missing from any of the homologs in cyanobacteria[17]. In contrast to chloroplasts, in cyanobacteria, photosynthetic and respiratory electron transport chains are both located in the same membrane system, the thylakoids, and even share some components[18]. Therefore, cyanobacteria cannot shut down ATP synthase as strictly as plant chloroplasts during the dark phase, since both the photosynthetic and respiratory electron chains generate proton gradients at the thylakoid membranes during day and night, respectively, which are used by the same ATP synthase for the generation of ATP[19]. Hence, the cyanobacterial ATP synthase complexes cannot be controlled by the same redox-sensitive mechanism as operating in the chloroplast.

Nevertheless, several mechanisms have been identified for the regulation of ATP synthase activity in cyanobacteria, the ADP-mediated inhibition that relies on the γ subunit[20] and ε subunit-mediated inhibition[21]. These findings provided hints that also mechanisms to prevent wasteful ATP hydrolysis activity of ATP synthase might exist in cyanobacteria.

Here, we provide evidence that a small protein previously called Norf1 (for novel ORF1) acts as ATP synthase regulator in cyanobacteria. Norf1 was initially discovered in the model cyanobacterium *Synechocystis* sp. PCC 6803 (*Synechocystis* 6803)

bioRxiv preprint doi: https://doi.org/10.1101/2021.07.30.454416; this version posted October 15, 2021. The copyright holder for this preprint (which was not certified by peer review) is the author/funder, who has granted bioRxiv a license to display the preprint in perpetuity. It is made available under aCC-BY-NC 4.0 International license.

based on the detection of its mRNA in transcriptomic datasets[22,23]. *Synechocystis* 6803 Norf1 comprises 48 amino acids, and its expression was confirmed at the protein level by Western blot analyses[24]. The *norf1* mRNA level was found to increase dramatically after the transfer of cultures into darkness[22]. Darkness-stimulated gene expression is very unusual in cyanobacteria, that base their physiology on light-dependent oxygenic photosynthesis. In *Synechocystis* 6803, only 62 out of a total of 4,091 experimentally defined transcriptional units exhibited maximum expression in the dark[22]. Therefore, it appeared elusive why a free-standing gene encoding a small protein of just 48 amino acids would be regulated in this way and make its transcript the mRNA with the highest absolute read count after 12 h in darkness[22].

To elucidate Norf1 function, we scrutinized its expression here in more detail, investigated mutant strains and identified interacting proteins. Norf1 is a soluble protein, but membrane fractionation experiments and fusions to GFP showed targeting to the thylakoid membrane. Immunoprecipitation followed by mass spectrometry and far Western blot suggested specific interactions with subunits of the ATP synthase complex. Finally, measurements of ATP hydrolysis in isolated membrane fractions, and purified ATP synthase complexes revealed that Norf1 is recruited during unfavorable conditions as an inhibitory subunit that prevents the hydrolysis of ATP. These findings prompted us to rename Norf1 and its gene to AtpΘ for the cyanobacterial ATP synthase inhibiTory factor (gene *atpT*).

bioRxiv preprint doi: https://doi.org/10.1101/2021.07.30.454416; this version posted October 15, 2021. The copyright holder for this preprint (which was not certified by peer review) is the author/funder, who has granted bioRxiv a license to display the preprint in perpetuity. It is made available under aCC-BY-NC 4.0 International license.

Results

Genes encoding homologs of AtpΘ are widely distributed throughout the cyanobacterial phylum

The 48 amino acid sequence of the previously identified *Synechocystis* 6803 Norf1 protein[24], here renamed AtpΘ, was used to search for homologs, resulting in the identification of highly similar proteins in 318 available cyanobacterial genomes, including all finished genomes and some of the permanent draft genomes (**Figure 1**). The occurrence, sequence and predicted isoelectric points of AtpΘ homologs are given in **Table S1**. These homologs were predicted based on quite short amino acid sequences; therefore, we cannot rule out that the list includes some false positives or that some homologs might have been missed. While most cyanobacterial genomes (228/318) possess a single *atpT* gene, we also identified 88 genomes with two and two genomes with three putative homologs (**Figure S1A**). Putative *atpT* homologs were not detected outside the cyanobacterial phylum, but homologs were found in two *Gloeobacter* species considered to represent the most ancestral clade[25], pointing at an early and stable acquisition of *atpT* in the cyanobacterial radiation (**Figure 1**). Most of the genomes containing two homologs are relatively large (median 6.23 Mb) and belong mainly to the genera *Fischerella, Calothrix, Scytonema* and *Nostoc*. The different copies in one strain are not identical, making their origin from recent gene duplications unlikely. The majority of the putative homologs are between 39 and 70 amino acids in length (**Figure S1B**), except those in *Halomicronema hongdechloris* C2206 and *Pseudanabaena* sp. PCC 7367 with 94 and 82 amino acids, respectively. However, the homolog in *Pseudanabaena* sp. PCC 7367 exhibits pronounced sequence similarity only within its central and C-terminal residues, potentially being

bioRxiv preprint doi: https://doi.org/10.1101/2021.07.30.454416; this version posted October 15, 2021. The copyright holder for this preprint (which was not certified by peer review) is the author/funder, who has granted bioRxiv a license to display the preprint in perpetuity. It is made available under aCC-BY-NC 4.0 International license.

translated from an internal start codon (marked in **Table S1** in red) and yielding a peptide of 51 residues.

AtpΘ homologs are predicted to be soluble proteins lacking transmembrane helices. Sequence comparison of selected AtpΘ homologs covering strains from all identified larger phylogenetic clusters among cyanobacteria showed quite different sequences, with only 7 widely conserved residues (**Figure S1C**). These residues include aromatic residues at positions 13 and 22, negatively charged residues at positions 16 and 27 and a conserved proline at position 30 with regard to the *Synechocystis* 6803 protein. This divergence is also reflected in the isoelectric points (IPs), which were predicted to range from acidic values (AtpΘ in *Synechocystis* 6803 and *Microcystis*) to very alkaline values (>11) for AtpΘ from thermophilic strains (**Table S1**).

Energy supply and proton gradient integrity impact *atpT* transcription

Northern blot experiments showed that the *atpT* transcript level increased within 10 min after transfer to darkness, rapidly reaching maximum values 30 min after transfer and declined only marginally at the latest time point (**Figure 2A**). The addition of 10 mM glucose neutralized the strong darkness-induced activation of gene expression (**Figure 2A**), suggesting that the stimulation of *atpT* transcript accumulation in the dark is connected to the energy supply for respiration. Based on these results, we chose an incubation time of 6 h in darkness for subsequent experiments. High *atpT* expression was also previously associated with transfer to darkness or low light conditions, entering stationary phase or heat shock[22,24]. We reasoned that all these conditions compromise photosynthetic activity and may affect the cellular redox status. Therefore, we tested additional conditions that interfere with the proton gradient or the electron transfer chain. Indeed, the parallel presence of the uncoupler carbonyl cyanide *m*-

bioRxiv preprint doi: https://doi.org/10.1101/2021.07.30.454416; this version posted October 15, 2021. The copyright holder for this preprint (which was not certified by peer review) is the author/funder, who has granted bioRxiv a license to display the preprint in perpetuity. It is made available under aCC-BY-NC 4.0 International license.

chlorophenyl hydrazone (CCCP)[26] or of the electron transport inhibitor 2,5-dibromo-3-methyl-6-isopropyl-*p*-benzoquinone (DBMIB)[27] restored the high transcript accumulation in the dark despite the addition of glucose (**Figure 2B**). These results indicated that it was not the lack of light *per se* that triggered *atpT* expression. Instead, the enhanced respiration fostered by the addition of glucose led to the suppression of the dark-induced increase in transcript accumulation, while CCCP or DBMIB lifted this suppression. We conclude that it was the potentially low capacity for ATP synthesis due to a diminished or absent proton gradient that triggered high *atpT* expression.

To evaluate the accumulation of the AtpΘ protein, a specific antibody was raised that detected a faint band with an apparent molecular mass of 8 kDa in samples from *Synechocystis* 6803 wild-type cultures grown in the dark but not in the light (**Figure 2C**). Expression of AtpΘ under the control of its native promoter from plasmid vector pVZ322 enhanced the detected band more than twofold, caused by the higher copy number of the plasmid-located gene. Western blot analysis also showed that AtpΘ started to accumulate 0.5 h after transfer to darkness and continued to become more abundant over a time period of 4 h, after which it remained at approximately the same level; transfer of the cultures back into light led to the disappearance of the AtpΘ signal within less than 4 h (**Figure 2D**). Thus, the time course of AtpΘ protein accumulation after transfer of cultures into darkness closely followed the time course of mRNA accumulation.

The inducibility by transfer into darkness might be characteristic of *atpT* expression and might support the identification of putative homologs in different species. We chose four species that are phylogenetically distant from *Synechocystis* 6803 (**Figure 1**). *Gloeobacter violaceus* PCC 7421 represents an early-branching species that lacks thylakoid membranes[28]. *Thermosynechococcus elongatus* BP-1

bioRxiv preprint doi: https://doi.org/10.1101/2021.07.30.454416; this version posted October 15, 2021. The copyright holder for this preprint (which was not certified by peer review) is the author/funder, who has granted bioRxiv a license to display the preprint in perpetuity. It is made available under aCC-BY-NC 4.0 International license.

belongs to a clade of unicellular thermophilic strains, while *Prochlorococcus* sp. MED4 is a laboratory isolate representing the vast marine picocyanobacterial genus *Prochlorococcus*[29]. Finally, *Nostoc* sp. PCC 7120 (*Nostoc* 7120) is a model strain for the group of heterocyst-differentiating and N_2-fixing multicellular cyanobacteria. The predicted AtpΘ homologs share as little as 12.5% (*Prochlorococcus* sp. MED4), 20.8% (*G. violaceus* PCC 7421), 33.3 and 41.4% (*T. elongatus* BP-1 and *Nostoc* 7120) identical amino acids with the *Synechocystis* 6803 protein. The results of Northern hybridizations showed that the predicted *atpT* homologs in all four strains were expressed at higher levels after 6 h in darkness than under light conditions (**Figures 2E** and **2F**). These findings reinforced the idea that these genes, identified only on the basis of sequence searches, might be orthologs of the *atpT* gene in *Synechocystis* 6803.

AtpΘ localizes in *Synechocystis* 6803 to soluble and membrane-enriched protein fractions

Strain P_{atpT}::*atpT*-3xFLAG was used to localize AtpΘ within soluble or membrane-enriched protein fractions. To verify the specificity of the Flag antibody, we also analyzed strains P_{atpT}::*atpT* (negative control) and P_{petJ}::3xFLAG-sf*gfp* (positive control). *Synechocystis* 6803 extracts from dark- and light-grown cultures were separated by centrifugation into membrane and soluble fractions and analyzed by Western blotting. FLAG-tagged proteins were detected in the respective lysates, while no signal was obtained for the negative control. AtpΘ was partitioned approximately equally between the soluble and membrane fractions, while FLAG-tagged sfGFP was restricted to the soluble fraction (**Figure 3A**). The FLAG tag stabilized the AtpΘ protein, since the FLAG-tagged version could be detected in samples from cultures kept under

bioRxiv preprint doi: https://doi.org/10.1101/2021.07.30.454416; this version posted October 15, 2021. The copyright holder for this preprint (which was not certified by peer review) is the author/funder, who has granted bioRxiv a license to display the preprint in perpetuity. It is made available under aCC-BY-NC 4.0 International license.

continuous light for 12 h, very different from the native form (**Figures 2C** and **2D**). We conclude that AtpΘ can associate with membranes despite the absence of a predicted membrane-spanning region.

Fusions to AtpΘ target GFP to the cyanobacterial thylakoid membrane

According to the fractionation analysis in *Synechocystis* 6803, AtpΘ localizes to soluble and membrane-enriched protein fractions, but it remained unclear if only to the thylakoids, the cellular inner or outer membrane, or several of them. To obtain insight into the possible subcellular localization of AtpΘ, we chose *Nostoc* 7120 because of its much larger cells than *Synechocystis* 6803. TblastN analyses indicated the presence of a single possible *atpT* homolog in a chromosomal region to which a transcriptional start site was previously assigned at position 2982087r[30]. Northern hybridization showed a transcript originating from this region (**Figure 2F**), consistent with the length of 316 nt predicted for this gene from the TSS to the end of a Rho-independent terminator[31]. The corresponding gene was classified as protein-coding[31] based on analysis by the RNAcode algorithm[32]. Upon shifting the cultures to darkness, this mRNA was rapidly induced (**Figure 2F**), similar to the regulation of the *atpT* gene in *Synechocystis* 6803 and three other cyanobacteria. Next, two constructs were prepared: pSAM342 harboring the *atpT* promoter, the corresponding 5'UTR plus the coding sequence for the green fluorescent protein (GFP) and pSAM344 harboring the *atpT* promoter, the 5'UTR, and the *atpT* coding region translationally fused to GFP (**Table S2**).

These constructs were introduced into plasmid α of *Nostoc* 7120 by homologous recombination. Confocal microscopy revealed GFP fluorescence in the recombinant strains obtained but not in a strain bearing a *gfp*-less control construct (**Figure 3B**).

bioRxiv preprint doi: https://doi.org/10.1101/2021.07.30.454416; this version posted October 15, 2021. The copyright holder for this preprint (which was not certified by peer review) is the author/funder, who has granted bioRxiv a license to display the preprint in perpetuity. It is made available under aCC-BY-NC 4.0 International license.

However, we noticed a distinct difference in the intracellular localization of the signal. The fluorescence of the cells expressing the transcriptional fusion from construct pSAM342 appeared distributed throughout the cytoplasm, i.e., typical for a soluble protein such as GFP (**Figure 3C**). In contrast, the fluorescence of the translational fusion pSAM344 was localized differently and appeared spatially associated with the thylakoid membrane system, indicated by the overlap between chlorophyll and GFP fluorescence signals (**Figure 3D**). We conclude that translational fusions between *atpT* and *gfp* were translated well and that the AtpΘ sequence was competent to direct GFP to the thylakoid membrane. This localization is consistent with the association of soluble AtpΘ with a thylakoid membrane-bound complex.

Interestingly, for both constructs, the signal was very low in those cells that exhibited no chlorophyll fluorescence (compare **Figure 3B** with **Figures 3C** and **3D**). These cells were heterocysts specialized for nitrogen fixation, the assimilation of nitrogen from dinitrogen gas, N_2, through the enzyme nitrogenase. This result provided evidence that the *atpT* promoter was switched off cell type-specifically in heterocysts.

ATP synthase subunits become enriched in coimmunoprecipitation experiments

To identify the function of AtpΘ, protein coimmunoprecipitation assays followed by mass spectrometry were conducted with protein extracts from *Synechocystis* 6803 cells expressing FLAG-tagged AtpΘ under the control of its native promoter (strain P_{atpT}::*atpT*-3xFLAG). As controls, a strain expressing untagged AtpΘ under control of the native promoter (strain P_{atpT}::*atpT*) and a strain expressing FLAG-tagged sfGFP controlled by the copper-regulated P_{petJ} promoter (strain P_{petJ}::3xFLAG-sf*gfp*) were used.

bioRxiv preprint doi: https://doi.org/10.1101/2021.07.30.454416; this version posted October 15, 2021. The copyright holder for this preprint (which was not certified by peer review) is the author/funder, who has granted bioRxiv a license to display the preprint in perpetuity. It is made available under aCC-BY-NC 4.0 International license.

The evaluation of pull-down experiments via mass spectrometry showed that 34 proteins, including eight subunits of F_oF_1 ATP synthase, were enriched with a log_2FC >3.5 among the proteins copurified with FLAG-tagged AtpΘ compared to at least one of the two controls (**Table S4**). These results pointed at a possible interaction between AtpΘ and one or several subunits of the F_oF_1 ATP synthase complex.

Two experiments were performed to verify this possibility. We performed a second immunoprecipitation assay comparing FLAG-tagged AtpΘ and FLAG-tagged sfGFP in three biological replicates each. The eluted samples were subjected to SDS-PAGE (**Figure S2**) and then analyzed using mass spectrometry. This analysis detected the same eight subunits of ATP synthase that were significantly enriched by coimmunoprecipitation with AtpΘ-3xFLAG (**Figure 4A**, marked in red), confirming the specific interaction between AtpΘ and the ATP synthase complex. Hence, in both analyses, the same 8 of the 9 known ATP synthase subunits were identified (**Tables S4** and **S5**). The only missing subunit was subunit c, the small membrane-intrinsic subunit, which appears to be difficult to detect by mass spectrometry. A small number of additional proteins significantly enriched by coimmunoprecipitation with AtpΘ-3xFLAG included two subunits of NAD(P)H-quinone oxidoreductase (subunit I and subunit O), two proteins of the CmpABCD transporter (CmpC and CmpA), and the bicarbonate transporter SbtA (**Figure 4B**), pointing at possible higher-order structures or additional binding partners of AtpΘ. The hierarchical clustering of AtpΘ-3xFLAG-enriched proteins labeled in **Figures 4A** and **4B**, as well as 3xFLAG-sfGFP is shown in **Figure 4C**. The resulting heat map further helped to visualize the enrichment of each protein, and the blank region under the 3xFLAG-sfGFP cluster indicates that no such proteins were identified. The complete dataset of the two independent

bioRxiv preprint doi: https://doi.org/10.1101/2021.07.30.454416; this version posted October 15, 2021. The copyright holder for this preprint (which was not certified by peer review) is the author/funder, who has granted bioRxiv a license to display the preprint in perpetuity. It is made available under aCC-BY-NC 4.0 International license.

coimmunoprecipitation assays can be obtained from the PRIDE partner repository (dataset identifiers PXD020126 and PXD024905).

As a further control experiment, we tested the enrichment of AtpB (subunit beta of ATP synthase) in an eluate from the pull-down experiment with FLAG-tagged AtpΘ by Western blotting. AtpB was clearly detected in this eluate but not in the eluate from the immunoprecipitation of 3xFLAG-sfGFP or a mock experiment with untagged AtpΘ (**Figure 4D**). Collectively, these results supported an interaction between AtpΘ and subunit(s) of the ATP synthase complex. Moreover, this interaction would explain the association of AtpΘ with thylakoid membranes as was observed in **Figure 3**.

Impact of AtpΘ on ATP synthase activity

The results in **Figure 3** showed that AtpΘ associates with thylakoid membranes and the results in **Figure 4** that it is the ATP synthase complex it is interacting with. To test its functional impact, the *atpT* gene was replaced by a chloramphenicol resistance cassette and biochemical measurements of ATPase activity were performed. Membrane fractions were isolated from both the wild type and the fully segregated *atpT* knockout strain (**Figure S1D),** which had been kept in continuous light or dark, and their ATP hydrolysis activities were analyzed. The results (**Figure 5A**) showed that the membrane fraction of wild-type *Synechocystis* 6803 grown in the light had a significantly higher ATPase activity than the membrane fraction isolated after 24 h of darkness incubation. In contrast, the membrane preparation from the knockout strain without AtpΘ showed no significant difference between the light- and dark-incubated conditions. These results suggested an *in vivo* inhibitory effect of AtpΘ on ATPase activity under darkness.

bioRxiv preprint doi: https://doi.org/10.1101/2021.07.30.454416; this version posted October 15, 2021. The copyright holder for this preprint (which was not certified by peer review) is the author/funder, who has granted bioRxiv a license to display the preprint in perpetuity. It is made available under aCC-BY-NC 4.0 International license.

Similar findings were observed in a second cyanobacterium, *Thermosynechococcus elongatus* BP-1, where the ATPase activities of the membrane samples prepared from light-cultivated cells were significantly higher than the ATPase activities of the membrane samples from dark-incubated cells (**Figure S3**). Thus, the predicted AtpΘ homolog of *Thermosynechococcus elongatus* BP-1 could function similarly to AtpΘ of *Synechocystis* 6803.

To further characterize the potential inhibitory effect of AtpΘ, the ATP hydrolysis activity of the membrane fraction from wild-type *Synechocystis* 6803 cells was measured in the presence of different amounts of an AtpΘ synthetic peptide (**Figure 5B**). The synthetic peptide AcnSP[33], which is of a length similar to AtpΘ and was synthesized by the same company, was used as negative control. In parallel, the well-established F_oF_1 ATP synthase inhibitor DCCD served as positive control. As shown in **Figure 5B**, AtpΘ reduced ATPase activity in a dose-dependent manner, and the inhibitory effect was saturated at 20 nmol AtpΘ, whereas the AcnSP peptide showed no effect on ATPase activity. High amounts of DCCD inhibited ATPase activity at a level similar to the AtpΘ peptide. Finally, the combination of DCCD and AtpΘ peptide yielded an ATPase inhibition similar to their separate addition. These results indicated that AtpΘ is a strong inhibitor of the ATP hydrolysis activity of F_oF_1 ATP synthase, comparable to DCCD. The remaining 60% ATP hydrolysis activity of the membrane preparations probably resulted from other ATP hydrolases, such as H^+-translocating P-type ATPases that are resistant to DCCD or PilT1 and PilB1 proteins providing energy for the type IV pili system[34,35], or because either AtpΘ or DCCD cannot fully inhibit ATPase activity. Then, to further confirm whether the difference between wild-type and knockout cells observed in **Figure 5A** was due to the lack of AtpΘ, 20 nmol of AtpΘ or AcnSP peptides was supplemented to the membrane isolated from the dark-

bioRxiv preprint doi: https://doi.org/10.1101/2021.07.30.454416; this version posted October 15, 2021. The copyright holder for this preprint (which was not certified by peer review) is the author/funder, who has granted bioRxiv a license to display the preprint in perpetuity. It is made available under aCC-BY-NC 4.0 International license.

incubated knockout strain. The results showed that supplementation with AtpΘ could significantly inhibit the ATPase activity of the membrane, while AcnSP showed no such effects (**Figure 5C**), further confirming the inhibitory role of AtpΘ.

To identify the minimal inhibitory sequence of AtpΘ and to study the effects of specific amino acids on the ATPase inhibitory effect of AtpΘ, four mutant AtpΘ peptides were designed and synthesized (**Figure S4**). The inhibitory effects of these peptides on ATPase activity were tested and compared to the inhibitory effects of the original AtpΘ peptide (**Figure 5D**). Interestingly, the N-terminal part of AtpΘ, which corresponds to the predicted alpha-helical part of this protein (peptide AtpΘ_N in **Figure 5D** and **Figure S4**), exhibited an inhibitory effect similar to that of? the entire peptide. In contrast, the central part of AtpΘ (AtpΘ_C in **Figure 5D** and **Figure S4**) showed weaker inhibitory effects. Introduction of two conserved amino acid substitutions (D26E and D27E) yielded AtpΘ_EE, as shown in **Figure 5D** and **Figure S4**. Consistent with the conservative replacement of two acidic residues by two others, a similar inhibitory effect on ATP hydrolysis activity was observed as for the native AtpΘ protein. In contrast, the introduction of a single histidine residue at this position (E27H; AtpΘ_H in **Figure 5D** and **Figure S4**) led to an almost complete loss of the inhibitory effect, indicating that the negative charge at this position is important for the inhibitory activity of the full-length AtpΘ peptide. The 3D structure modeling of AtpΘ using PEP-FOLD3[36] and analysis using the HELIQUEST web server[37] predicted an N-terminal amphipathic alpha helix and a C-terminal random structure, which was also observed in the predicted structures of representative AtpΘ homologs from cyanobacteria strains with one, two or three putative homologs (**Figure S5**). These results suggest that the N-terminal alpha helix of AtpΘ is a conserved structural

bioRxiv preprint doi: https://doi.org/10.1101/2021.07.30.454416; this version posted October 15, 2021. The copyright holder for this preprint (which was not certified by peer review) is the author/funder, who has granted bioRxiv a license to display the preprint in perpetuity. It is made available under aCC-BY-NC 4.0 International license.

element that is together with the cluster of centrally located, negatively charged amino acids responsible for the inhibition of ATPase activity.

F_0F_1 ATP synthase purification and the effect of AtpΘ

To rule out the effects of membrane proteins other than ATP synthase, ATP synthase was purified from *Synechocystis* 6803 cells by fusing a 3xFLAG tag to the C-terminus of AtpB. The purified protein complex was first characterized by SDS-PAGE, showing good purity and distribution of different subunits (**Figure 6A**), and then probed using anti-FLAG and anti-AtpB antisera (**Figures 6B** and **6C**, respectively), confirming the presence of both 3xFLAG and AtpB. The ATPase activity of the purified ATP synthase was then measured directly or in the presence of different inhibitors (**Figure 6D**). ATP hydrolysis activity was detected using the purified protein complex. Compared with the purified complex, the addition of AcnSP peptide yielded no significant changes, whereas the addition of AtpΘ peptide or DCCD significantly decreased the ATPase activity. The inhibitory effect of AtpΘ appeared stronger than the inhibitory effect of DCCD, and the combination of both showed no additive effects. These results further confirmed the inhibitory effect of the AtpΘ peptide on the hydrolytic activity of ATP synthase.

Far Western blot identifies interaction partners of AtpΘ from purified ATP synthase

To gain further insight into the interaction between AtpΘ and the ATP synthase complex, a far Western blot approach[38] was applied. In this approach, proteins were renatured after blotting onto a membrane and served as baits. The membrane was

bioRxiv preprint doi: https://doi.org/10.1101/2021.07.30.454416; this version posted October 15, 2021. The copyright holder for this preprint (which was not certified by peer review) is the author/funder, who has granted bioRxiv a license to display the preprint in perpetuity. It is made available under aCC-BY-NC 4.0 International license.

then incubated with the synthetic AtpΘ peptide, followed by anti-AtpΘ serum and anti-rabbit IgG antiserum. As shown in **Figure 6E-G**, AtpΘ was enriched mainly at two positions, which were assigned as subunit a (*atpB*, Sll1322) and subunit c (*atpE*, Ssl2615), respectively, based on the comparison to the subunit distribution of *E. coli* F_0F_1 ATP synthase[39]. A very weak signal of approximately 50 kDa size was also observed, which should correspond to subunit alpha or subunit beta (**Figure 6G)**. Although the 50 kDa signal was relatively weak, it was reproducibly observed (n = 3) and should therefore also be considered. As a negative control, a mock far Western blot was conducted in which TBST buffer was used instead of the synthetic AtpΘ peptide. In this setting, no signal was observed for the two replicates of ATP synthase purification, while the positive controls could be detected (**Figure S6**), suggesting that none of the signals observed in **Figures 6E and 6G** were due to unspecific interaction with any of the antisera used. These results further confirmed the specific interaction of the AtpΘ peptide with distinct subunits of ATP synthase.

Discussion

F_0F_1-type ATP synthases produce ATP via chemiosmotic coupling to a proton gradient. However, while ATP synthases preferentially catalyze ATP formation, a weaker or temporarily missing proton gradient can stimulate the reverse reaction, pumping protons while hydrolyzing ATP. In the mitochondria of yeast and mammals, small inhibitory peptides can prevent ATP synthase from running backwards, hence avoiding wasteful ATP hydrolysis. In plant chloroplasts, in which the proton gradient is generated by light-driven photosynthetic electron transport, a redox-controlled mechanism switches ATP synthase activity off at night when photosynthesis does not take place[1]. In this respect, cyanobacteria present an interesting case because

bioRxiv preprint doi: https://doi.org/10.1101/2021.07.30.454416; this version posted October 15, 2021. The copyright holder for this preprint (which was not certified by peer review) is the author/funder, who has granted bioRxiv a license to display the preprint in perpetuity. It is made available under aCC-BY-NC 4.0 International license.

photosynthetic ATP synthesis is light-driven, as in chloroplasts, but conditions can easily be envisioned where inhibition of ATP hydrolysis is warranted. Such conditions can be low light, darkness and others that would affect the strength of the proton gradient. Cellular ATP demand is likely considerably lower under certain conditions, e.g., during the night, but in contrast to chloroplasts, residual activity should be maintained in cyanobacteria to allow respiration to proceed with ATP synthesis, which uses the same ATP synthase that is also used for photosynthesis in the thylakoid membrane system.

Several mechanisms have been identified for regulating ATP synthase activity in cyanobacteria (**Figure 7**). A common regulatory mechanism, the ADP-mediated inhibition of the F_1 part, has been reported for cyanobacterial ATPase[20]. Although the γ subunit of cyanobacteria is not redox-sensitive compared to the chloroplast F_0F_1 ATP synthase subunit γ, the ADP-mediated inhibition of ATPase was assigned to this subunit[20]. Another well-characterized mechanism is the inhibition of the rotation of bacterial F_0F_1 ATP synthase via the ε subunit, called ε inhibition[40]. ε inhibition in cyanobacteria was reported to be ATP-independent, different from other bacteria, and was related to the distinct γ subunit of cyanobacteria as well[41]. In addition, both the γ and ε subunits of cyanobacterial F_0F_1 ATP synthase were reported to be important for the dark acclimation of cyanobacteria[21]. However, many aspects of the regulation of cyanobacterial F_0F_1 ATP synthase have remained unknown.

In the present study, we suggest that the small protein AtpΘ represents a functional analog in cyanobacteria of the small inhibitory peptides that arrest ATP synthase from running backwards in mitochondria. This hypothesis is supported by several lines of evidence. First, the direct interaction of AtpΘ with ATP-synthase subunits has been shown in different protein/protein interaction studies, where it

bioRxiv preprint doi: https://doi.org/10.1101/2021.07.30.454416; this version posted October 15, 2021. The copyright holder for this preprint (which was not certified by peer review) is the author/funder, who has granted bioRxiv a license to display the preprint in perpetuity. It is made available under aCC-BY-NC 4.0 International license.

437 showed the strongest binding toward subunit a (*atpB*, Sll1322) and subunit c (*atpE*,
438 Ssl2615) (**Figure 6G**). Second, AtpΘ supplementation had a specific, dose-dependent
439 negative impact on ATP hydrolysis activity in isolated membrane fractions or using the
440 purified ATP synthase complex. The extent of this inhibition was similar to the inhibition
441 exerted by specific ATP synthase inhibitors, consistent with its role in preventing the
442 reverse reaction, i.e., the wasting of ATP via hydrolysis when the proton gradient is
443 weakened. The addition of synthetic Atpθ peptide to the membrane samples prepared
444 from *Synechocystis* 6803 cultured in the presence of light yielded a maximum 35%
445 inhibition of ATPase activity (**Figure 5B**). A slightly higher inhibitory effect of 40% was
446 achieved if Atpθ peptide was added to the preparations of purified ATP synthase
447 (**Figure 6D**). These findings indicate that the Atpθ peptide may inhibit up to 40% of the
448 ATPase activity in ATP synthase. Third, investigations of wild type and *atpT* mutant
449 strains are consistent with the *in vitro* ATP synthase activity tests. While the membrane
450 sample prepared from *Synechocystis* 6803 cultured under continuous light showed a
451 similar ATPase activity as previously reported[21], the membrane samples prepared from
452 dark-incubated *Synechocystis* 6803 with maximum *atpT* expression showed an
453 ATPase activity of approximately 85% (**Figure 5A**), and this difference was not
454 observed in the *atpT* knock-out mutant of *Synechocystis* 6803, indicating that the Atpθ
455 protein is required *in vivo* to decrease ATPase activity during dark incubation. Fourth,
456 the expression data suggest that the AtpΘ action is controlled mostly via the regulation
457 of its expression because the protein seems to have a low stability (**Figure 2D**). Its
458 expression is particularly stimulated under conditions that could weaken the
459 transmembrane proton gradient, such as darkness, or, in our experiments, by the
460 addition of the uncoupler CCCP or the electron chain inhibitor DBMIB (**Figure 2B**).
461 While CCCP is a well-established protonophore, DBMIB is better known as an inhibitor

bioRxiv preprint doi: https://doi.org/10.1101/2021.07.30.454416; this version posted October 15, 2021. The copyright holder for this preprint (which was not certified by peer review) is the author/funder, who has granted bioRxiv a license to display the preprint in perpetuity. It is made available under aCC-BY-NC 4.0 International license.

of photosynthetic electron transfer. However, DBMIB affects the cytochrome b_6f complex[27], which is shared by photosynthetic and respiratory electron transfer that operates in the same membrane system in cyanobacteria. In contrast, the presence of AtpΘ might be futile when ATP synthase runs at high speed, such as under high-light conditions driven by an efficient photosynthetic light reaction or in the presence of high rates of respiration. Consistently, *atpT* dark induction could largely be prevented by the addition of glucose (**Figure 2A**), likely due to the stimulation of respiration-dependent ATP synthesis in the presence of glucose. Furthermore, such a scenario of high respiration exists in heterocysts, which have no photosystem II but exhibit substantial ATP production to meet the high demand of nitrogen-fixing nitrogenase, linked to high rates of respiration consuming the O_2 inside the heterocysts. Indeed, we observed that the expression of the *atpT* promoter was shut down in heterocysts of *Nostoc* 7120 (**Figure 3C** and **3D**). Finally, the cross-phylum importance of the AtpΘ-mediated prevention of the backward reaction of ATP synthase is supported by its ubiquitous occurrence throughout the cyanobacterial phylum and our finding that *atpT* expression was stimulated under conditions leading to lowered thylakoid proton gradients in several divergent species of cyanobacteria (**Figure 2E** and **2F**). These results make it very likely that the conclusions obtained with the model *Synechocystis* 6803 can also be generalized for other cyanobacteria.

Collectively, these data provide evidence that the small protein AtpΘ acts as an ATP hydrolysis inhibitor of cyanobacterial ATP synthase. This role of AtpΘ represents an interesting analogy to the ATP synthase regulator IF1 in the mitochondria of eukaryotes. However, unlike IF1, which binds the catalytic interface between the α and β subunits[42], the main potential interaction partners of AtpΘ, subunits a and c, belong to the F_0 part of ATP synthase, which resides within the thylakoid membrane (**Figure**

bioRxiv preprint doi: https://doi.org/10.1101/2021.07.30.454416; this version posted October 15, 2021. The copyright holder for this preprint (which was not certified by peer review) is the author/funder, who has granted bioRxiv a license to display the preprint in perpetuity. It is made available under aCC-BY-NC 4.0 International license.

7). The predicted amphipathic character of the N-terminal helix in AtpΘ homologs (**Figure S5C**) may support the interaction with membrane proteins such as subunits a and c but may facilitate also additional interactions with subunits in the soluble phase. Therefore, the binding of AtpΘ to the two topographically close subunits a and c and its amphipathic character point to a possibly divergent mechanism of AtpΘ function by hindering the rotation of the ATP synthase complex through direct binding.

Acknowledgments

This study was funded by the German Research Foundation (DFG) priority program SPP2002 “Small Proteins in Prokaryotes, an Unexplored World” (grant HE 2544/12-1 to WRH, grant HA 2002/22-1 to MH and grant BE 3869/5-1 to DöB), by grant PID2019-105526GB-I00/AEI/10.13039/501100011033 (AEI/FEDER, UE) to AMMP, and by a China Scholarship Council grant to K.S. We thank the ZBSA proteomics staff, especially Verónica I. Dumit, for support, Gen Enomoto, for an aliquot of *Thermosynechococcus elongatus* BP1, Mai Watanabe for an aliquot of *Gloeobacter violaceus* PCC 7421 and Claudia Steglich for a culture of *Prochlorococcus* sp. MED4 (all University of Freiburg).

Author contributions

KS and DeB carried out the molecular-genetic and biochemical analyses in *Synechocystis* 6803, and AMMP performed all experiments in *Nostoc* 7120. SM and DöB performed proteomics analyses. MH provided scientific input for improving the experimental design and physiological interpretation. WRH designed the study, and all

bioRxiv preprint doi: https://doi.org/10.1101/2021.07.30.454416; this version posted October 15, 2021. The copyright holder for this preprint (which was not certified by peer review) is the author/funder, who has granted bioRxiv a license to display the preprint in perpetuity. It is made available under aCC-BY-NC 4.0 International license.

authors analyzed the data. KS and WRH drafted the manuscript. All authors read and approved the final manuscript.

Declaration of interests

The authors declare that they have no competing interests.

bioRxiv preprint doi: https://doi.org/10.1101/2021.07.30.454416; this version posted October 15, 2021. The copyright holder for this preprint (which was not certified by peer review) is the author/funder, who has granted bioRxiv a license to display the preprint in perpetuity. It is made available under aCC-BY-NC 4.0 International license.

Main text Figures

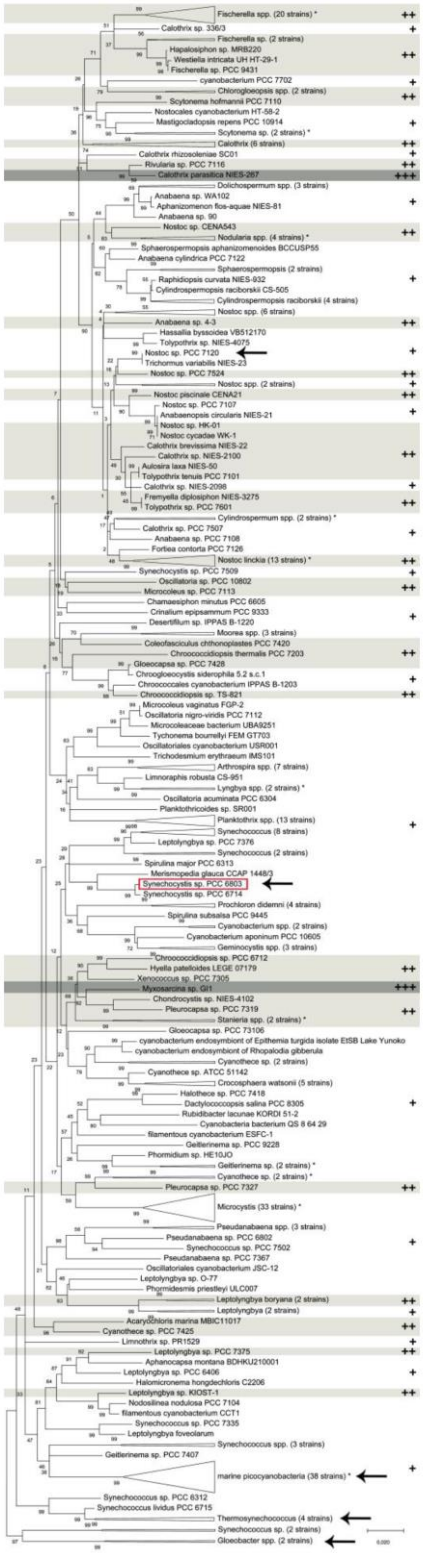

516

Figure 1. Distribution and numbers of *atpT* genes throughout the cyanobacterial phylum. Phylogenetic tree of cyanobacteria based on 16S rRNA sequences (SILVA database[43] constructed in MEGAX[44] using the minimum evolution method[45]). The number of individual strains is given in brackets if several strains were joined at one

bioRxiv preprint doi: https://doi.org/10.1101/2021.07.30.454416; this version posted October 15, 2021. The copyright holder for this preprint (which was not certified by peer review) is the author/funder, who has granted bioRxiv a license to display the preprint in perpetuity. It is made available under aCC-BY-NC 4.0 International license.

branch (e.g., 33 strains for *Microcystis*), marine picocyanobacteria consisting of *Prochlorococcus* and marine *Synechococcus*. The numbers of putative *atpT* homologs in each strain are indicated (+, one; ++, two; +++, three homologs) and additionally highlighted in shades of gray if more than one. Single deviations within clusters of strains joined at one branch are labeled by asterisks (e.g., among the 20 *Fischerella* spp. strains in the uppermost cluster is one strain with one homolog, while all others have two). Species selected for experimental analyses in this study are labeled by arrows, and the location of the *Synechocystis* 6803 model strain is additionally highlighted by a red box. The optimal tree with the sum of branch length = 5.06878059 is shown. The percentage of replicate trees in which the associated taxa clustered together in the bootstrap test (500 replicates) is shown next to the branches[46]. The tree is drawn to scale, with branch lengths in the same units as the units of the evolutionary distances used to infer the phylogenetic tree. The analysis involved 318 nucleotide sequences. All ambiguous positions were removed for each sequence pair (pairwise deletion option). There were a total of 1753 positions in the final dataset. The sequences of all potential AtpΘ homologs are given in **Table S1**.

bioRxiv preprint doi: https://doi.org/10.1101/2021.07.30.454416; this version posted October 15, 2021. The copyright holder for this preprint (which was not certified by peer review) is the author/funder, who has granted bioRxiv a license to display the preprint in perpetuity. It is made available under aCC-BY-NC 4.0 International license.

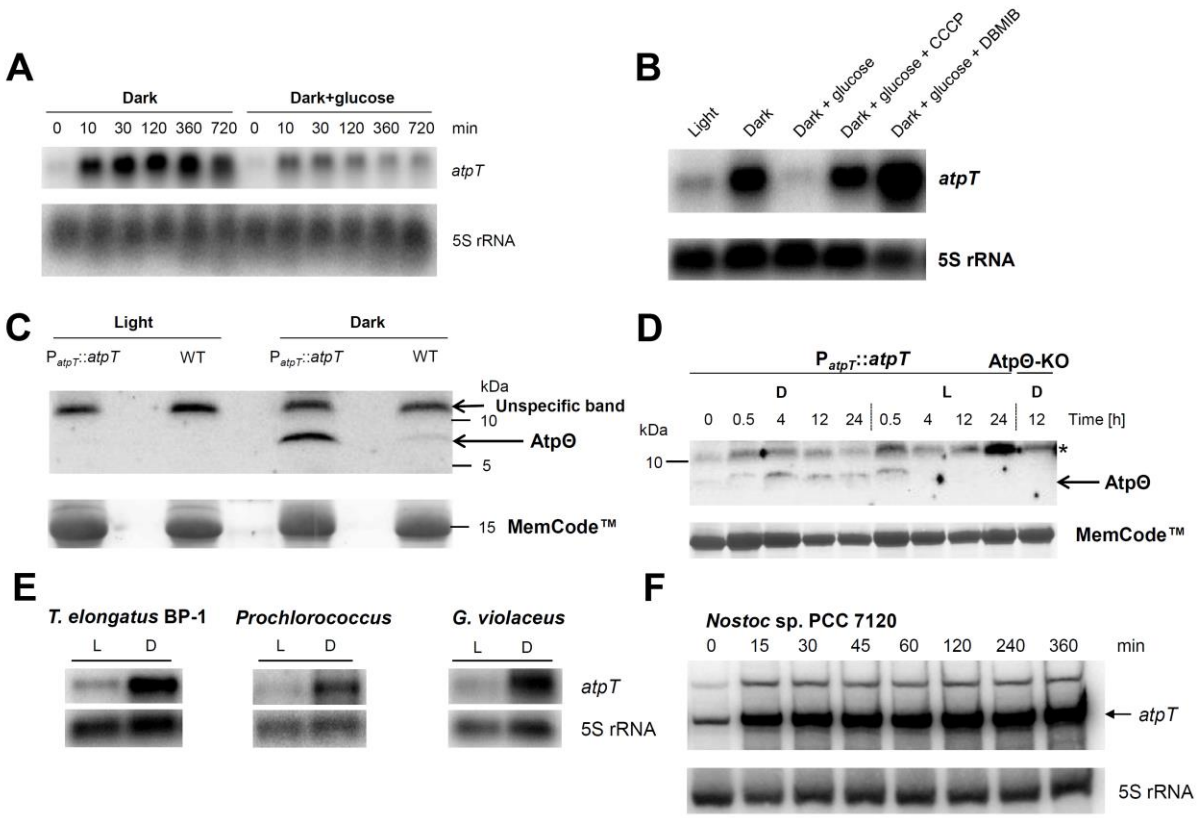

Figure 2. Expression of *atpT* is stimulated by low energy, uncoupling or inhibition of electron transfer. (A) Time course of *atpT* mRNA accumulation in the dark in the presence or absence of glucose (10 mM). Exponentially growing *Synechocystis* 6803 wild-type (WT) cells were harvested at the indicated time points before and after transfer to darkness. Northern hybridization was carried out after separation and blotting of 1 µg of total RNA with a ^{32}P-labeled, single-stranded transcript probe specifically recognizing *atpT*. **(B)** *atpT* mRNA accumulation after 6 h under the indicated conditions and treatments. CCCP and DBMIB were added to final concentrations of 10 µM and 100 µM, respectively. **(C)** Western blot experiment for the detection of native AtpΘ. Protein levels were compared in *Synechocystis* 6803 WT cells and in cultures carrying the P_{atpT}::*atpT* construct in which the untagged *atpT* gene was overexpressed from its native promoter on the plasmid vector pVZ322 in addition to the native gene copy. Identical amounts of 150 µg total protein were separated by Tricine SDS-PAGE[47] and probed with anti-AtpΘ serum after transfer to nitrocellulose membrane. Precision Plus Protein™ DualXtra (2-250 kDa, Bio-Rad) was used as molecular mass marker. The same membrane was stained with MemCode™ as a loading control. **(D)** AtpΘ expression under changing light conditions. Samples for protein extraction were collected at the indicated time points. Approximately 150 µg (calculated according to Direct Detect™ Spectrometer measurements) of protein samples was separated. PageRuler™ Prestained Protein Ladder (10–170 kDa, Fermentas) was used as molecular mass marker. MemCode™ staining served as a loading control. D, darkness, L, standard light (~40 µmol photons m^{-2} s^{-1}), AtpΘ-KO, AtpΘ knockout (only last lane). In panels **(C)** and **(D)**, the position of untagged AtpΘ is indicated, * indicates a strong cross-reacting band. **(E)** Northern analysis of potential

bioRxiv preprint doi: https://doi.org/10.1101/2021.07.30.454416; this version posted October 15, 2021. The copyright holder for this preprint (which was not certified by peer review) is the author/funder, who has granted bioRxiv a license to display the preprint in perpetuity. It is made available under aCC-BY-NC 4.0 International license.

atpT homologs in *Thermosynechococcus elongatus* BP-1, *Prochlorococcus* sp. MED4, and *Gloeobacter violaceus* PCC 7421. For each sample, 5 µg of total RNA was loaded. L, strains were cultured in constant light; D, light-cultured strains were incubated in darkness for 6 h. **(F)** Time course of *atpT* mRNA accumulation in *Nostoc* 7120 in cultures transferred from light to darkness for the indicated times. In panels (A), (B), (E) and (F) the respective 5S rRNA was hybridized as a loading control.

bioRxiv preprint doi: https://doi.org/10.1101/2021.07.30.454416; this version posted October 15, 2021. The copyright holder for this preprint (which was not certified by peer review) is the author/funder, who has granted bioRxiv a license to display the preprint in perpetuity. It is made available under aCC-BY-NC 4.0 International license.

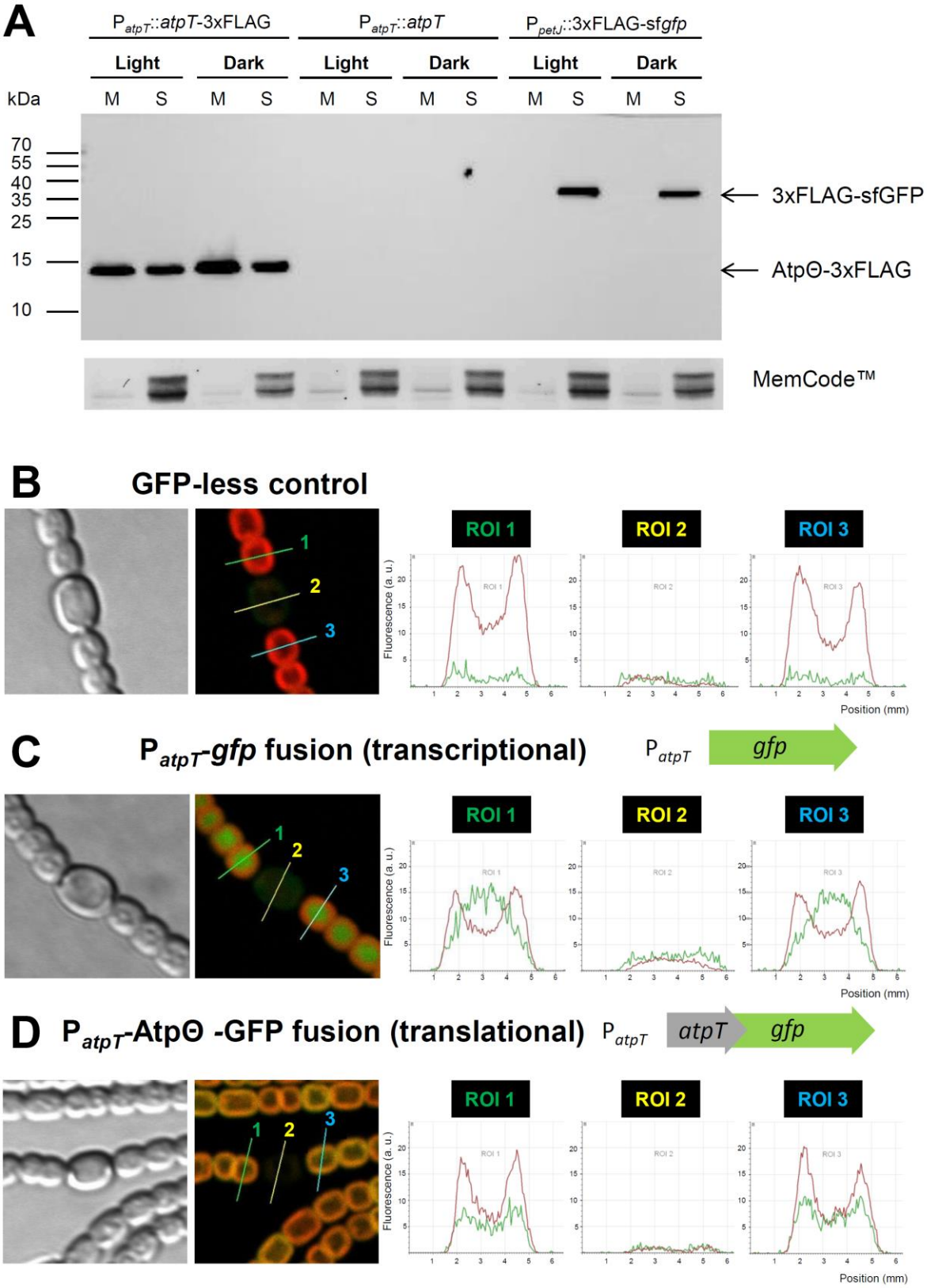

Figure 3. Intracellular localization of AtpΘ. (A) Localization of FLAG fusion proteins by separation of the membrane fraction from soluble proteins. Samples for protein extraction were taken from light- and dark (12 h incubation)-grown cultures of *Synechocystis* 6803 mutant strains: P_{atpT}::*atpT*-3xFLAG and P_{petJ}::3xFLAG-sf*gfp* expressed the recombinant AtpΘ and Gfp-FLAG fusion proteins, respectively, whereas

bioRxiv preprint doi: https://doi.org/10.1101/2021.07.30.454416; this version posted October 15, 2021. The copyright holder for this preprint (which was not certified by peer review) is the author/funder, who has granted bioRxiv a license to display the preprint in perpetuity. It is made available under aCC-BY-NC 4.0 International license.

P_{atpT}::*atpT* was used as a negative control. Proteins (10 µg) were separated on a 15% (w/v) glycine SDS polyacrylamide gel and transferred to a nitrocellulose membrane, which was probed with specific ANTI-FLAG® M2-Peroxidase (HRP) antibody. MemCode™ Reversible Protein staining was used to check for equal protein loading. M, membrane fraction, S, soluble fraction. **(B) to (D)** Fluorescence-based analysis of the localization of AtpΘ in *Nostoc* 7120 bearing different fusions to GFP. **(B)** GFP-less control. **(C)** Transcriptional fusion: The *gfp* gene was placed under the control of the *atpT* promoter (construct pSAM342, **Table S2**). **(D)** Translational fusion: The *gfp* gene was fused to the *atpT* coding region and placed under the control of the *atpT* promoter (pSAM344, **Table S2**). In panels **(B)** to **(D)**, first, light transmission microscopy is shown, followed by fluorescence in the GFP channel merged with chlorophyll autofluorescence. The following three diagrams show the fluorescence intensities in cross sections region of interest (ROI) 1 to ROI 3 in three consecutive single cells, two vegetative cells and one heterocyst in the middle. GFP fluorescence is depicted in green, and chlorophyll autofluorescence is depicted in red.

bioRxiv preprint doi: https://doi.org/10.1101/2021.07.30.454416; this version posted October 15, 2021. The copyright holder for this preprint (which was not certified by peer review) is the author/funder, who has granted bioRxiv a license to display the preprint in perpetuity. It is made available under aCC-BY-NC 4.0 International license.

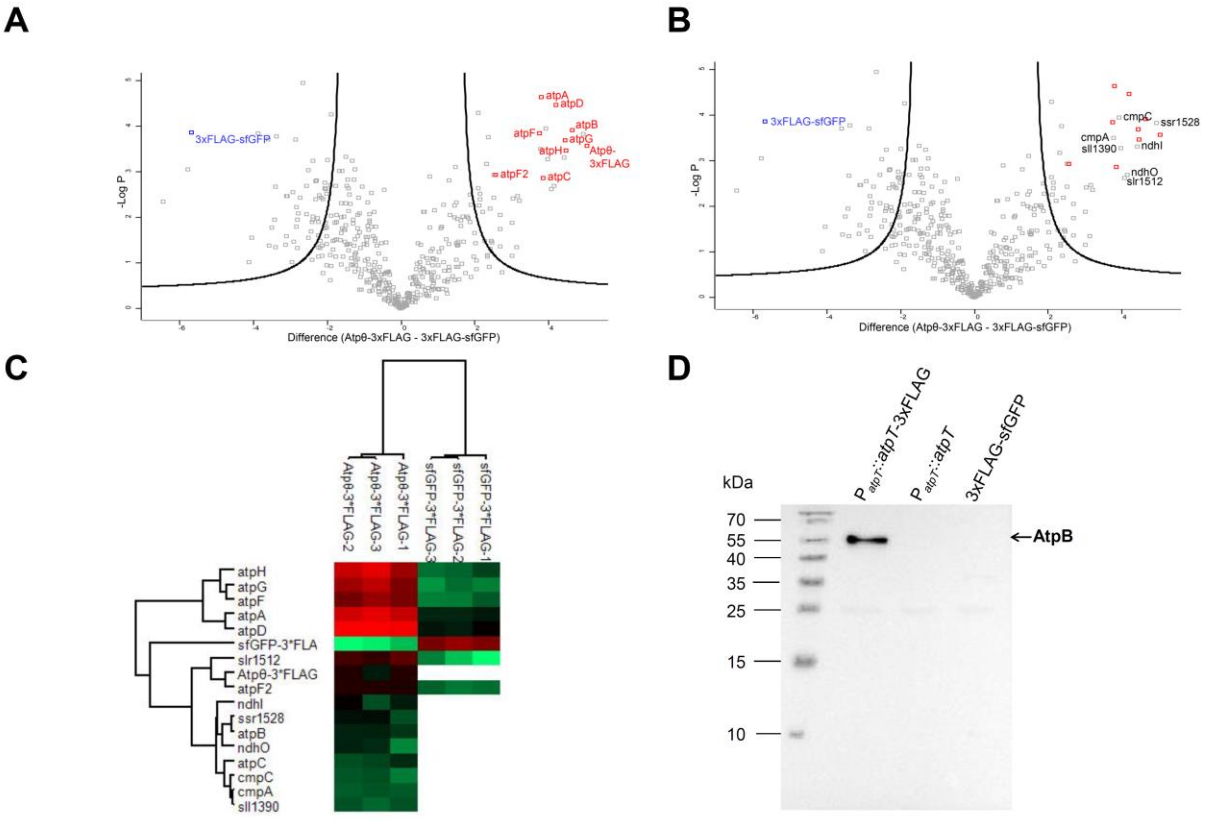

Figure 4. Copurification of AtpΘ and the ATP synthase complex verified by mass spectrometry and immunoblot analysis. (A) Volcano plot generated based on a two-sample *t*-test of enriched proteins using a false discovery rate (FDR) of 0.01 and a coefficient for variance minimization s_0 [48] of 2. Atpθ-3xFLAG and the identified subunits of F_0F_1 ATP synthase are marked in red, while 3xFLAG-GFP is marked in blue. Subunit b' (AtpF2) was added manually to the plot since this subunit was detected in only 2 out of 3 replicates. **(B)** The same volcano plot shown in **(A)** labeled with non-ATP synthase proteins. **(C)** Clustering heat map of the Atpθ-3xFLAG-enriched proteins marked in volcano plots (**A** and **B**). The $\log_2$ transformed NSAF intensities are indicated by different colors as indicated below. Undetected proteins in the 3xFLAG-GFP-enriched samples were left blank. 3xFLAG-GFP was detected in the Atpθ-3xFLAG group due to their common 3xFLAG tag. **(D)** Probing the elution fractions of P_{atpT}::*atpT*-3xFLAG, P_{atpT}::*atpT* and P_{petJ}::3xFLAG-sf*gfp* with anti-AtpB serum.

520

bioRxiv preprint doi: https://doi.org/10.1101/2021.07.30.454416; this version posted October 15, 2021. The copyright holder for this preprint (which was not certified by peer review) is the author/funder, who has granted bioRxiv a license to display the preprint in perpetuity. It is made available under aCC-BY-NC 4.0 International license.

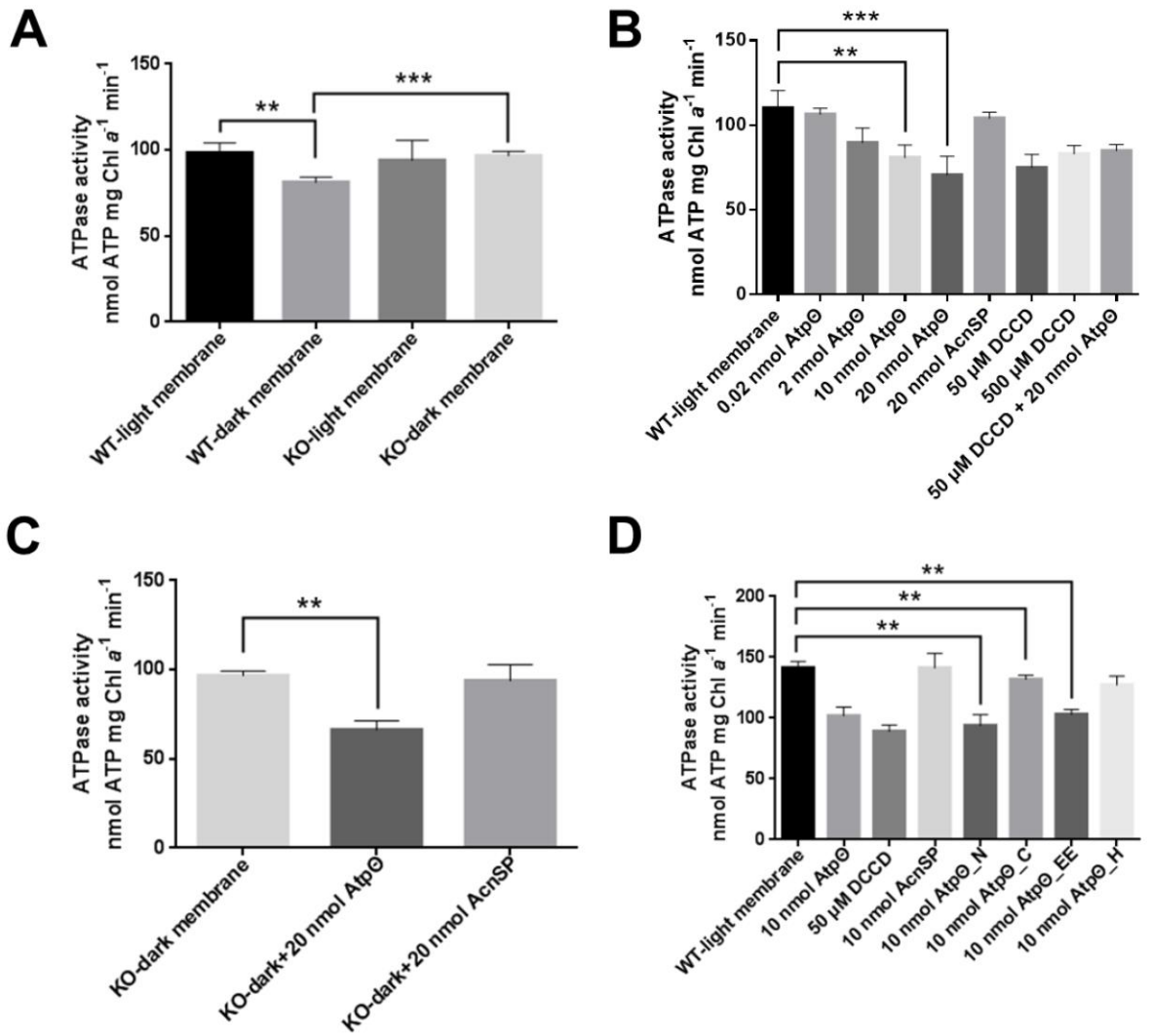

Figure 5. ATPase activities in membrane fractions. (A) ATPase activity of the membrane fraction of wild type and *atpT* knockout *Synechocystis* 6803 cells growing under continuous light or after 24 hours of darkness incubation. **(B)** ATPase activity of the membrane fraction of wild-type *Synechocystis* 6803 supplemented with different synthetic peptides or chemicals. DCCD was used as a positive control for ATPase activity inhibition, while the synthetic AcnSP peptide was used as a negative control. **(C)** ATPase activity of the membrane fraction isolated from *atpT* knockout *Synechocystis* 6803 cells after 24 hours of darkness incubation supplemented with either synthetic AtpΘ or AcnSP peptide. **(D)** ATPase inhibitory effects of AtpΘ peptides with truncated or modified sequences (**Figure S4**). The differences between groups were tested using GraphPad software as described in the methods section. Significance was established at $P < 0.05$ = ** and $P < 0.01$ = ***.

521

bioRxiv preprint doi: https://doi.org/10.1101/2021.07.30.454416; this version posted October 15, 2021. The copyright holder for this preprint (which was not certified by peer review) is the author/funder, who has granted bioRxiv a license to display the preprint in perpetuity. It is made available under aCC-BY-NC 4.0 International license.

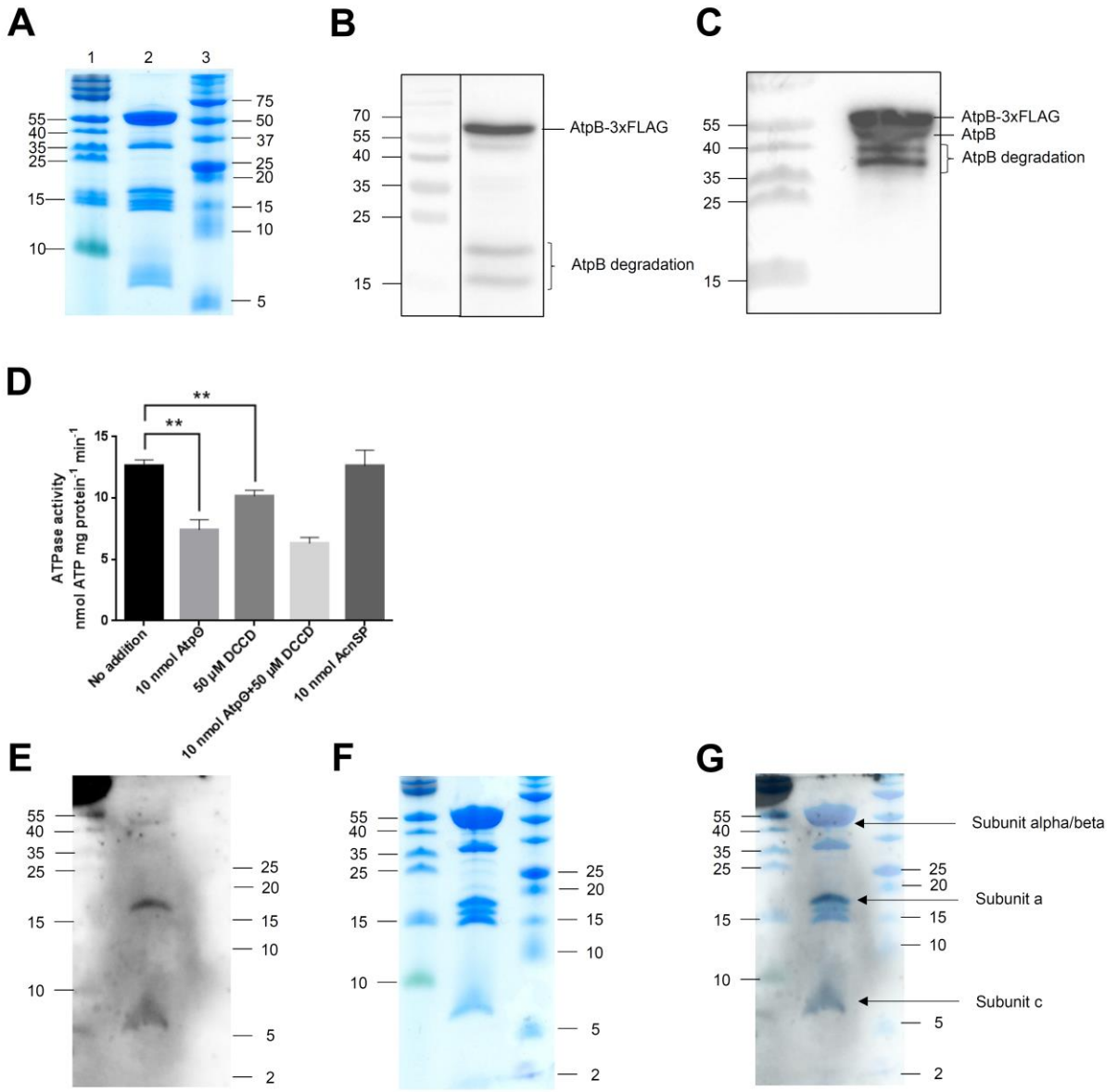

Figure 6. Purification of the F_0F_1 ATP synthase and its interaction with AtpΘ. (A) Tricine SDS-PAGE displaying the purity of 10 µg *Synechocystis* 6803 F_0F_1 ATP synthase (lane 2) isolated with AtpB-3xFLAG and gel filtration chromatography. PageRuler™ Prestained Protein Ladder (lane 1; 10 to 180 kDa) and Precision Plus Protein™ Dual Xtra Prestained Protein Standard (lane 3; 2 to 250 kDa) were used as molecular mass markers. **(B)** Western blot analysis of 10 µg purified *Synechocystis* 6803 F_0F_1 ATP synthase probed with specific ANTI-FLAG® M2-Peroxidase (HRP) antibody. **(C)** Western blot analysis of 10 µg purified *Synechocystis* 6803 F_0F_1 ATP synthase probed with anti-AtpB serum. The doublet for AtpB consists of the native and 3xFLAG-tagged forms of the protein. Bands in panels b and c likely resulting from degradation are labeled. **(D)** Measurement of the ATP hydrolysis activity of purified F_0F_1 ATP synthase supplemented with different synthetic peptides or chemicals. DCCD was used as a positive control for ATPase activity inhibition, while the synthetic AcnSP peptide was used as a negative control. The differences between groups were

bioRxiv preprint doi: https://doi.org/10.1101/2021.07.30.454416; this version posted October 15, 2021. The copyright holder for this preprint (which was not certified by peer review) is the author/funder, who has granted bioRxiv a license to display the preprint in perpetuity. It is made available under aCC-BY-NC 4.0 International license.

tested using a paired *t*-test (**Table S10**) using GraphPad software. Significance was established at **, $P < 0.05$. **(E)** Far Western blot signal detecting the interaction partners of synthetic AtpΘ peptide from purified *Synechocystis* 6803 F_0F_1 ATP synthase. **(F)** Coomassie blue staining of the Tricine-SDS gel after blotting. **(G)** The immunoblot signal (**E**) was merged with the stained gel (**F**) to determine the interacting subunits. The subunits suspected to interact with Atpθ are labeled. PageRuler™ Prestained Protein Ladder (10–170 kDa, Fermentas; left) and Protein™ DualXtra (2-250 kDa, Bio-Rad; right) were used as molecular mass markers. In total, 15 µg purified ATP synthase was loaded on the gel.

bioRxiv preprint doi: https://doi.org/10.1101/2021.07.30.454416; this version posted October 15, 2021. The copyright holder for this preprint (which was not certified by peer review) is the author/funder, who has granted bioRxiv a license to display the preprint in perpetuity. It is made available under aCC-BY-NC 4.0 International license.

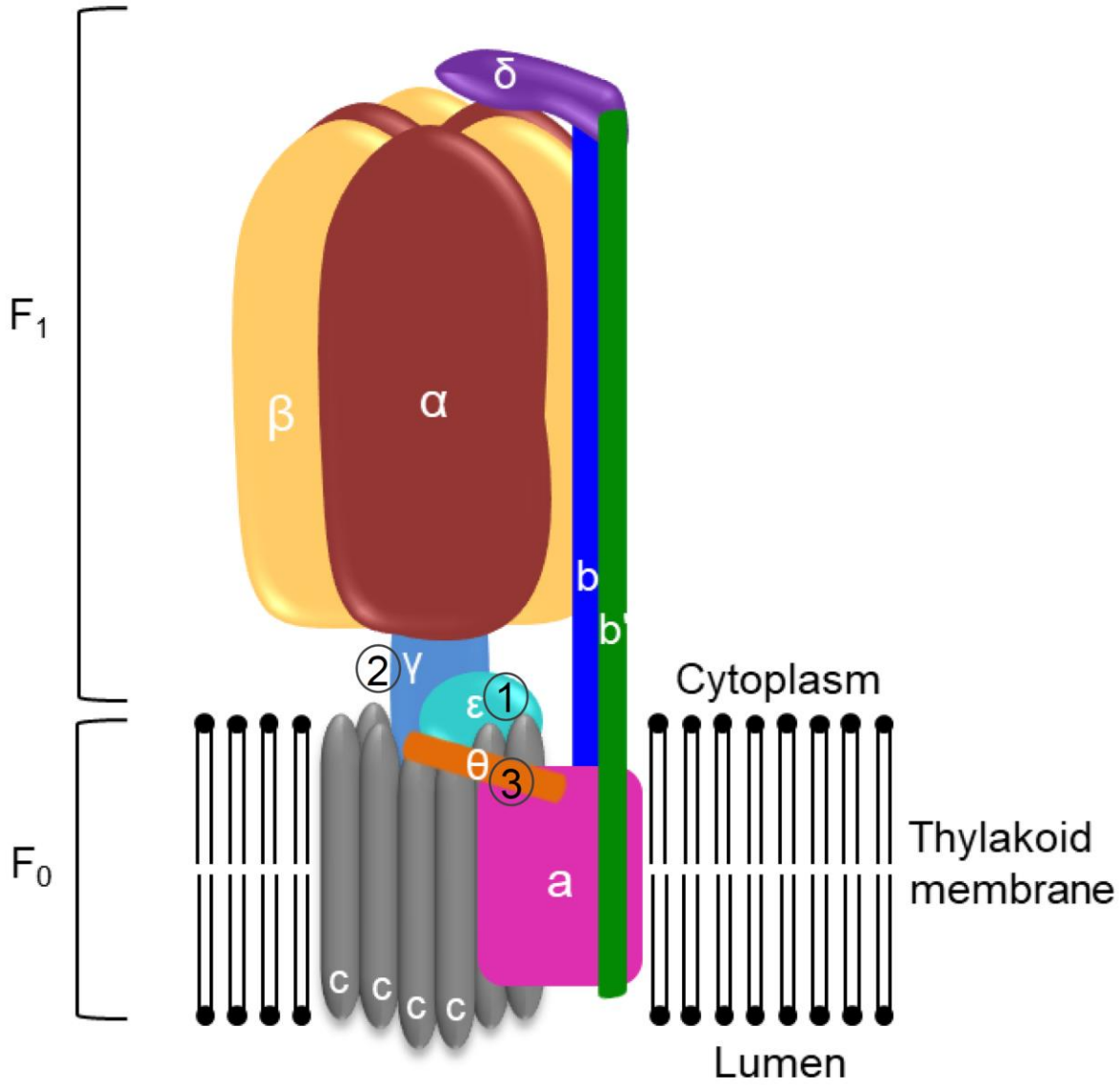

Figure 7. Regulatory and inhibitory mechanisms impacting hydrolysis of ATP by ATP synthases in cyanobacteria. (1) ε–inhibition[21], a mechanism in which the ε subunit inhibits the rotation of the γ subunit via a conformational change[41]; (2) ADP inhibition, the most conserved mechanism to block ATPase activity (reviewed by Lapashina and Feniouk[49]) via a segment inserted in the γ subunit[20], or (3) by AtpΘ. In this suggested mechanism, H^+ ions pass through the c ring and drive its rotation, and then the upper part of the complex rotates together in the non-inhibited state. AtpΘ may block the rotation of the c ring via interaction with subunit a. The computationally predicted structure of AtpΘ has tentatively been drawn next to subunits a and c, but the exact topography and mode of interaction with these membrane-embedded subunits is a topic of future research.

523

bioRxiv preprint doi: https://doi.org/10.1101/2021.07.30.454416; this version posted October 15, 2021. The copyright holder for this preprint (which was not certified by peer review) is the author/funder, who has granted bioRxiv a license to display the preprint in perpetuity. It is made available under aCC-BY-NC 4.0 International license.

STAR Methods

RESOURCE AVAILABILITY

Lead contact

Further information and requests for resources and reagents should be directed to and will be fulfilled by the lead contact, Wolfgang R. Hess (wolfgang.hess@biologie.uni-freiburg.de).

Materials availability

N/A

Data and code availability

- Mass spectrometry raw data have been deposited at the ProteomeXchange Consortium (http://proteomecentral.proteomexchange.org) and are publicly available as of the date of publication. Accession numbers are listed in the key resources table.
- This paper does not report original code.
- Any additional information required to reanalyze the data reported in this paper is available from the lead contact upon request.

EXPERIMENTAL MODEL AND SUBJECT DETAILS

Cultivation of cyanobacteria

Wild-type *Synechocystis* sp. PCC 6803 PCC-M and mutant strains were cultured photoautotrophically in TES-buffered (20 mM, pH 8.0) BG11 medium[50] with gentle agitation or on agar-solidified (1.5% Kobe I agar) plates under constant illumination with white light of approximately 40 µmol photons m^{-2} s^{-1} at 30°C and supplemented

bioRxiv preprint doi: https://doi.org/10.1101/2021.07.30.454416; this version posted October 15, 2021. The copyright holder for this preprint (which was not certified by peer review) is the author/funder, who has granted bioRxiv a license to display the preprint in perpetuity. It is made available under aCC-BY-NC 4.0 International license.

with appropriate antibiotics (5 µg/mL gentamicin, 10 µg/mL kanamycin, and 3 µg/mL chloramphenicol). For incubation in darkness, flasks were wrapped with aluminum foil. $CuSO_4$ (2 µM) was used to induce the expression of the Cu^{2+}-responsive *petE* promoter[51], while the *petJ* promoter was induced by removing Cu^{2+} from the medium through centrifugation and resuspension. For high-density cultivation used for ATP synthase purification, *Synechocystis* 6803 overexpressing P_{petE}-*atpB*-3xFLAG was cultured in the cell-DEG system as reported previously[52] using freshwater medium[53] with the following modifications: Na_2EDTA and $CuSO_4$ were not included in the medium, and 10 µg/mL kanamycin or 5 µg/mL gentamicin was added.

Cultures of *Nostoc* 7120 were bubbled with an air/CO_2 mixture (1% v/v) and grown photoautotrophically at 30°C in BG11 medium[50]. Darkness was implemented on air-CO_2-bubbled cultures by covering with aluminum foil plus black velvet. The thermophilic cyanobacterium *Thermosynechococcus elongatus* BP-1 was cultured in BG11 medium under continuous illumination with 30 µmol photons m^{-2} s^{-1} white light (Master LED tube Universal 1200 mm UO 16 W830 T8; Philips) at 45°C. *Gloeobacter violaceus* PCC 7421 was cultivated photoautotrophically in Allen's medium[54] in Erlenmeyer flasks under continuous white light (4 µmol photons m^{-2} s^{-1}) at 20°C with shaking. *Prochlorococcus* MED4 cells were grown at 22°C in AMP1 medium[55] under 30 µmol photons m^{-2} s^{-1} continuous white cool light and harvested in an exponential growth phase.

METHOD DETAILS

Construction of mutant cyanobacterial strains

To delete the *atpT* gene from *Synechocystis* 6803 (genome position 3274499 to 3274645, reverse strand), the flanking regions of *atpT* were amplified by primer pairs AtpTKO-up-F/AtpTCmKO-up-R and AtpTCmKO-down-F/AtpTKO-down-R, and the

bioRxiv preprint doi: https://doi.org/10.1101/2021.07.30.454416; this version posted October 15, 2021. The copyright holder for this preprint (which was not certified by peer review) is the author/funder, who has granted bioRxiv a license to display the preprint in perpetuity. It is made available under aCC-BY-NC 4.0 International license.

resulting fragments were fused with a chloramphenicol resistance cassette and a pUC19 backbone amplified with primer pairs AtpTKO-vec-F/AtpTKO-vec-R and CmR-F/CmR-R using AQUA cloning[56]. The resulting plasmid, pUC-atpTKO-CmR, was then transferred into wild-type *Synechocystis* 6803 by natural transformation. The transformants were selected on BG11 agar plates supplemented with chloramphenicol. Complete segregation was achieved after several rounds of selection.

The construction of overexpression strains P_{atpT}::*atpT*, P_{atpT}::*atpT*-3xFLAG, and P_{petJ}::3xFLAG-sf*gfp* was described previously [24]. P_{petE}::*atpB*-3xFLAG, a strain overexpressing the FLAG-tagged subunit AtpB, was constructed using primer pairs pUC19-XbaI_PpetE_fw/atpB::PpetE_rev, PpetE::atpB_fw/3xFlag_atpB_rev and atpB_3xFlag_fw/3xFlag_PstI-pUC19_rev. The primers used for mutant construction are listed in **Table S3**.

Construction of *Nostoc* 7120 strains. The strain carrying plasmid pCSEL24 (*gfp*-less control) was constructed previously[57]. To construct pSAM342 (transcriptional fusion of coordinates 2982431 to 2982070 from *Nostoc* 7120, reverse strand), a PCR fragment was amplified with oligonucleotides 900+901, *Cla*I-*Xho*I-digested and cloned into *Cla*I-*Xho*I-digested pSAM270[58]. To generate pSAM344 (translational Atpθ-GFP fusion, coordinates 2982431 to 2981902, reverse strand), a PCR fragment was amplified with oligonucleotides 900+902, *Cla*I-*EcoR*V-digested and cloned into *Cla*I-*EcoR*V-digested pSAM147[59] in frame with the *gfpmut2* gene, rendering pSAM343. The *EcoR*I fragment from pSAM343, containing the fusion between the *atpT* promoter, the *atpT* gene and the *gfpmut2* gene, was cloned into *EcoR*I-digested pCSEL24, rendering pSAM344. All plasmids were transferred by conjugation followed by selection of

bioRxiv preprint doi: https://doi.org/10.1101/2021.07.30.454416; this version posted October 15, 2021. The copyright holder for this preprint (which was not certified by peer review) is the author/funder, who has granted bioRxiv a license to display the preprint in perpetuity. It is made available under aCC-BY-NC 4.0 International license.

streptomycin/spectinomycin (5 µg/mL each)-resistant colonies after integration in the alpha megaplasmid.

Computational sequence analyses

Homologs of the *atpT* gene were searched using the *Synechocystis* 6803 AtpΘ as query against the IMG[60] and UniProt databases using blastP and against the NCBI database using both TblastN[61] and blastP[62] at a threshold E value ≤$1e^{-5}$. Multiple sequence alignments were conducted using Jalview2[63]. Isoelectric points were predicted by the R package pIR[64].

Phylogenetic analyses were conducted in MEGA X[44] using the maximum likelihood algorithm based on 16S rRNA sequences extracted from the SILVA database[43] and modified according to Klähn *et al*.[65]. The evolutionary distances were computed using the maximum composite likelihood method[66].

Fluorescence microscopy

Images of *Nostoc* 7120 filaments growing on top of nitrogen-free solid media were taken five days after plating. The accumulation of GFP was analyzed and quantified using a Leica TCS SP2 confocal laser scanning microscope as previously described[67].

Protein extraction and Western blots

Synechocystis 6803 cells for protein extraction were harvested by centrifugation (4,000 x g, 10 min, 4°C) and resuspended in PBS buffer (137 mM NaCl, 2.7 mM KCl, 10 mM Na_2HPO_4, 1.8 mM KH_2PO_4, pH 7.4) containing protease inhibitor cocktail. Cells were then disrupted mechanically in a Precellys homogenizer (Bertin Technologies). Glass beads and unbroken cells were removed by centrifugation at 1,000 g for 1 min at 4°C, and the total crude protein was obtained. Before loading, protein samples were boiled

bioRxiv preprint doi: https://doi.org/10.1101/2021.07.30.454416; this version posted October 15, 2021. The copyright holder for this preprint (which was not certified by peer review) is the author/funder, who has granted bioRxiv a license to display the preprint in perpetuity. It is made available under aCC-BY-NC 4.0 International license.

with 1x protein loading buffer at 95°C for 10 min or incubated at 50°C for 30 min supplemented with 2% SDS if the membrane fraction was included.

For Western blot analysis, proteins were separated either in 15% glycine-SDS gels or in 16%/6 M urea Tricine-SDS gels. PageRuler Prestained Protein Ladder (10–170 kDa, Fermentas) or Precision Plus Protein DualXtra (2–250 kDa, Bio-Rad) was used as a molecular mass marker. The separated proteins were then transferred to nitrocellulose membranes (Hybond™-ECL, GE Healthcare) by semidry electroblotting. The blotted membrane was then blocked with 3% skimmed milk dissolved in TBST (20 mM Tris pH 7.6, 150 mM NaCl, 0.1% Tween-20) and incubated with primary antibody (1:500 dilution for anti-AtpΘ antiserum and 1:2,000 for anti-AtpB antibody) and secondary antibody (1:10,000 anti-rabbit antibody) sequentially. The anti-AtpΘ antiserum was generated by a commercial provider (Pineda Antikörper-Service). Signals were detected with ECL start Western blotting detection reagent (GE Healthcare) on a chemiluminescence imager system (Fusion SL, Vilber Lourmat).

Isolation of FLAG-tagged proteins and mass spectrometry analysis

For the pull-down assay, 800 mL of *Synechocystis* 6803 culture at an OD_{750} of approximately 1 was harvested by centrifugation at 4,000 g for 30 min at 4°C. Cell pellets were washed once with prechilled FLAG buffer (50 mM Hepes-NaOH pH 7.0, 5 mM $MgCl_2$, 25 mM $CaCl_2$, 150 mM NaCl, 10% glycerol, 0.1% Tween-20) and then resuspended in the same buffer supplemented with protease inhibitor cocktail. The cell suspension was disrupted with a Precellys homogenizer (Bertin Technologies, France). All subsequent steps were carried out at 4°C. Total cell extracts and glass beads were transferred to Bio-Spin® Disposable Chromatography Columns (Bio-Rad), which were put on centrifugation tubes (Sorvall Instruments). The glass beads were separated from cellular components by centrifugation (4,000 g, 5 min, 4°C). Membrane

bioRxiv preprint doi: https://doi.org/10.1101/2021.07.30.454416; this version posted October 15, 2021. The copyright holder for this preprint (which was not certified by peer review) is the author/funder, who has granted bioRxiv a license to display the preprint in perpetuity. It is made available under aCC-BY-NC 4.0 International license.

644 proteins were then solubilized by adding 2% *n*-dodecyl-beta-D-maltoside (β-DM),
645 followed by dark incubation for 1 h at 4°C with gentle agitation. Nonsoluble components
646 were removed by centrifugation (25,000 g, 30 min, 4°C), and the solubilized crude
647 extract (sCE) was transferred to a new tube.

648 FLAG-tagged proteins were purified by column chromatography using ANTI-
649 FLAG M2 affinity agarose gel or ANTI-FLAG M2 magnetic beads (both from Sigma-
650 Aldrich) according to the manufacturer's instructions. When ANTI-FLAG M2 affinity
651 agarose gel was used, the sCE was loaded and passed over the column three times
652 to improve binding. The column was washed with 5 x 2 mL of FLAG buffer, and the
653 FLAG-tagged proteins were eluted by incubating the matrix with 1x protein loading
654 buffer at 50°C for 30 min. The agarose was sedimented by centrifugation (16,000 g, 5
655 min, RT), and 20 µL of the resulting eluates were loaded on a glycine SDS-PAGE,
656 which was subsequently stained with Coomassie. Then, each gel lane was cut into
657 pieces, destained, desiccated and rehydrated in trypsin as previously described[68]. In
658 gel-digest was incubated at 37 °C overnight and peptides were eluted with water by
659 sonication for 15 min.

660 Samples were loaded on an EASY-nLC II system (Thermo Fisher Scientific)
661 equipped with an in-house built 20 cm column (inner diameter 100 µm, outer diameter
662 360 µm) filled with ReproSil-Pur 120 C18-AQ reversed-phase material (3 µm particles,
663 Dr. Maisch GmbH). Elution of peptides was achieved with a nonlinear 77 min gradient
664 from 1 to 99% solvent B (0.1% (v/v) acetic acid in acetonitrile) with a flow rate of 300
665 nl/min and injected online into an LTQ Orbitrap XL (Thermo Fisher Scientific). The
666 survey scan at a resolution of R=30,000 and 1 x 10^6 automatic gain control target in
667 the Orbitrap with activated lock mass correction was followed by selection of the five
668 most abundant precursor ions for fragmentation. Single charged ions as well as ions

bioRxiv preprint doi: https://doi.org/10.1101/2021.07.30.454416; this version posted October 15, 2021. The copyright holder for this preprint (which was not certified by peer review) is the author/funder, who has granted bioRxiv a license to display the preprint in perpetuity. It is made available under aCC-BY-NC 4.0 International license.

without detected charge states were excluded from MS/MS analysis. Fragmented ions were dynamically excluded from fragmentation for 30 s. Database searches with Sorcerer-SEQUEST 4 (Sage-N Research, Milpitas, USA) were performed against a *Synechocystis* 6803 database downloaded from Uniprot (Proteome-ID UP000001425) on 11/12/20, which was supplemented with common laboratory contaminants and the sequences of AtpΘ-3xFLAG and GFP-3xFLAG. After adding reverse entries the final database contained 7,102 entries. Database searches were based on a strict trypsin digestion with two missed cleavages permitted. No fixed modifications were considered and oxidation of methionine was considered as variable modification. The mass tolerance for precursor ions was set to 10 ppm and the mass tolerance for fragment ions to 0.5 Da. Validation of MS/MS-based peptide and protein identification was performed with Scaffold V4.8.7 (Proteome Software, Portland, USA), and peptide identifications were accepted if they exhibited at least deltaCn scores of greater than 0.1 and XCorr scores of greater than 2.2, 3.3 and 3.75 for doubly, triply and all higher charged peptides, respectively. Protein identifications were accepted if at least 2 unique peptides were identified.

Volcano plot visualization of the mass spectrometry results was performed using Perseus (version 1.6.1.3)[69] according to the following procedures. Contaminants and proteins with less than three valid values in at least one experimental group (Atpθ-3xFLAG and GFP-3xFLAG) were first removed from the matrix, and the normalized spectrum abundance factor (NSAF) intensities were $\log_2$-transformed. Imputation of the missing values was then performed based on the normal distribution of each column using default settings. Two sample *t* tests were performed before generating the final volcano plot. A heat map was generated by the hierarchical clustering function of Perseus 1.6.1.3 with default settings.

bioRxiv preprint doi: https://doi.org/10.1101/2021.07.30.454416; this version posted October 15, 2021. The copyright holder for this preprint (which was not certified by peer review) is the author/funder, who has granted bioRxiv a license to display the preprint in perpetuity. It is made available under aCC-BY-NC 4.0 International license.

694 FLAG-tagged F_0F_1 ATP synthase was purified from *Synechocystis* 6803
695 overexpressing P_{petE}::*atpB*-3xFLAG using a similar approach with modifications.
696 *Synechocystis* 6803 overexpressing P_{petE}::*atpB*-3xFLAG was cultured in Cu^{2+}-free
697 medium using the cell-DEG system in which much higher optical densities were
698 obtained[52]. Cu^{2+} at 2 µM was added to the system when the OD_{750} reached 8.0 to
699 induce the expression of the *petE* promoter, and the cells were collected by
700 centrifugation (5,000 g, 10 min, room temperature). Cell pellets were washed once
701 using prechilled FLAG buffer 2 (FLAG buffer without Tween-20). After disruption using
702 Precellys (all remaining steps were performed at 4°C unless stated otherwise), the
703 lysate was centrifuged at 4,000 g for 10 min to remove unbroken cells and beads,
704 followed by 20,000 g for 1 h to collect the membrane fraction. The membrane fraction
705 was then resuspended in FLAG buffer 2 supplemented with 1% *n*-dodecyl-beta-D-
706 maltoside (β-DM) and incubated for 1 h with gentle agitation. Nonsoluble components
707 were removed by centrifugation (20,000 g, 30 min), and the supernatant was filtered
708 with a 0.45 µm syringe filter and then subjected to ANTI-FLAG M2 affinity agarose gel
709 electrophoresis. The resin was prepared according to the manufacturer's instructions
710 using FLAG buffer 3 (FLAG buffer 2 supplemented with cocktail protease inhibitor and
711 0.03% [w/v] β-DM). The column was washed with 5 x 2 mL FLAG buffer 3 and eluted
712 with 1.5 mL FLAG buffer 3 with 150 µg/mL 3xFLAG peptide (Sigma-Aldrich). The
713 eluates were then concentrated to 200 µl with a 100 kDa MWCO centrifuge
714 concentrator. The protein concentration was measured using the Bradford method.

715 ***RNA isolation and Northern blot***

716 Cyanobacterial cells except those of *Nostoc* 7120 were harvested by vacuum filtration
717 on hydrophilic polyethersulfone filters (Pall Supor®-800; 0.8 µm for *Synechocystis*
718 6803, *Thermosynechococcus elongatus* BP-1 and *Gloeobacter violaceus* PCC 7421,

bioRxiv preprint doi: https://doi.org/10.1101/2021.07.30.454416; this version posted October 15, 2021. The copyright holder for this preprint (which was not certified by peer review) is the author/funder, who has granted bioRxiv a license to display the preprint in perpetuity. It is made available under aCC-BY-NC 4.0 International license.

719 0.45 µm for *Prochlorococcus* MED4). Total RNA was then isolated using PGTX[70]. The
720 isolated RNA was mixed with 2x loading buffer (Ambion) and incubated for 5 min at
721 65°C. Denatured RNA samples were separated in a 1.5% agarose gel supplemented
722 with 16% (v/v) formaldehyde and then transferred to a positively charged nylon
723 membrane (Hybond™-N+, GE Healthcare) by capillary blotting with 20x SSC buffer (3
724 M NaCl, 0.3 M sodium acetate, pH 7.0) overnight.

725 After the RNA was cross-linked to the membrane by UV light (125 mJ), the
726 membranes were hybridized with specific [γ-^{32}P]ATP end-labeled oligonucleotides or
727 [α-^{32}P]UTP-labeled single-stranded RNA probes generated by *in-vitro* transcription
728 from DNA templates using the MAXIscript® T7 In Vitro Transcription Kit (Ambion). The
729 primers and oligonucleotides used for generating DNA templates are given in **Table**
730 **S3**. Hybridization in 0.12 M sodium phosphate buffer (pH 7.0), 7% SDS, 50% deionized
731 formamide and 0.25 M NaCl was performed overnight at 45°C or at 62°C with labeled
732 oligonucleotide probes or labeled transcript probes, respectively. The hybridized
733 membrane was then washed using washing solutions I (2xSSC, 1% SDS), II (1x SSC,
734 0.5% SDS) and III (0.1x SSC, 0.1% SDS) for 10 min each at 5 degrees below the
735 hybridization temperature. Total RNA from *Nostoc* 7120 was prepared as described[71]
736 and separated on 8% urea-acrylamide gels. As a probe, a PCR fragment was
737 generated as template to label one strand with Taq polymerase using only one
738 oligonucleotide and [α-^{32}]P-dCTP. Signals were visualized using Typhoon FLA 9500
739 (GE Healthcare) or Cyclone Storage Phosphor System (PerkinElmer) and Quantity
740 One® software (Bio-Rad).

741 ***Membrane preparation and ATP hydrolysis assay***

742 One liter of *Synechocystis* 6803 or *Thermosynechococcus elongatus* BP-1 cultures
743 were grown to an OD_{750} of approximately 1 and cells were collected by centrifugation

bioRxiv preprint doi: https://doi.org/10.1101/2021.07.30.454416; this version posted October 15, 2021. The copyright holder for this preprint (which was not certified by peer review) is the author/funder, who has granted bioRxiv a license to display the preprint in perpetuity. It is made available under aCC-BY-NC 4.0 International license.

744 at 6,000 g for 5 min. The pellet was then washed once with precooled buffer A (1.0 M
745 betaine, 0.4 M d-sorbitol, 20 mM HEPES-NaOH, 15 mM $CaCl_2$, 15 mM $MgCl_2$, 1 mM
746 6-amino-*n*-caproic acid, and protease inhibitor cocktail; pH 7.0) and then lysed using a
747 Precellys homogenizer (steps afterwards were conducted at 4°C). Glass beads and
748 unbroken cells were removed by centrifugation at 4,000 g for 10 min, and then the
749 crude membranes were collected by centrifugation at 20,000 g for 1 h. The acquired
750 membrane pellet was washed twice with buffer A, resuspended and incubated on ice
751 for at least 1 h. Undissolved components were removed by centrifugation at 4,000 g
752 for 5 min, and the membrane suspension was quantified by measuring the Chl *a*
753 concentration at OD_{664}[72].

754 The ATPase activity of the membrane was measured via an ATP hydrolysis
755 coupled enzyme activity assay. Buffer B (10 mM TES, 100 mM KCl, 1 mM $MgCl_2$, and
756 0.1 mM $CaCl_2$; pH 7.5) was supplemented with the indicated amounts of synthetic
757 peptide or DCCD at room temperature. Then, 1 mM Mg-PEP, 0.175 mM NADH, 65 U
758 pyruvate kinase (PK) and 82.5 U lactate dehydrogenase (LDH) was added. Before the
759 activity measurement, 1 mM MgATP (pH 7.5) solution was added and incubated for 1
760 min to remove residual ADP. Then, membrane preparations containing approximately
761 10 μg Chl *a* were added to each assay, and the OD_{340} was measured immediately and
762 after 10 min of incubation at room temperature using quartz cuvettes. The ATPase
763 activity was calculated accordingly at nmol ATP mg Chl a^{-1} min^{-1}. For the measurement
764 of ATPase activity of the isolated ATP synthase, a similar method was applied, and 20
765 μg protein was used for each assay.

766 ***Far Western blotting***

767 Far Western blotting was performed as described previously[38,73] with modifications.
768 After electrophoresis, proteins were transferred onto a PVDF membrane. Synthetic

bioRxiv preprint doi: https://doi.org/10.1101/2021.07.30.454416; this version posted October 15, 2021. The copyright holder for this preprint (which was not certified by peer review) is the author/funder, who has granted bioRxiv a license to display the preprint in perpetuity. It is made available under aCC-BY-NC 4.0 International license.

AtpΘ peptide, anti-AtpΘ antiserum and anti-rabbit IgG antiserum were used for incubation sequentially. Milk powder was omitted in the denaturing/renaturing steps of the blotted membrane as described by Krauspe *et al*.[73]. The membrane with renatured proteins was first blocked with 5% milk powder in TBS-T and then incubated with 3 µg/mL synthetic AtpΘ peptide at 4°C overnight. Signals were detected with ECL start Western blotting detection reagent (GE Healthcare) on a chemiluminescence imager system (Fusion SL, Vilber Lourmat).

QUANTIFICATION AND STATISTICAL ANALYSIS

Statistical analyses were performed with GraphPad Prism 6.0 (GraphPad Software, Inc., San Diego, CA). The ATP hydrolysis activities of membrane fractions isolated from different strains or conditions were compared using unpaired *t*-test with Welch's correction (**Figure 5A** and **Figure S3; Data S1A** and **S1F**), and those of membranes isolated from the same strain but with different additives were compared using ratio paired *t*-test (**Figures 5A, 5B, 5C, 5D** and **Figure 6D; Data S1A, S1B, S1C, S1D** and **S1E**). Differences between groups were considered to be significant at a *P* value of <0.05 and very significant at a *P* value of <0.01.

KEY RESOURCES TABLE

REAGENT or RESOURCE	SOURCE	IDENTIFIER
Antibodies		
Mouse anti-FLAG M2 antibody	Sigma-Aldrich	Cat#A8592-1MG
Polyclonal AtpB antiserum | Beta subunit of ATP synthase (chloroplastic + mitochondrial; rabbit antibodies)	Agrisera, Sweden	Cat# AS05 085-10

bioRxiv preprint doi: https://doi.org/10.1101/2021.07.30.454416; this version posted October 15, 2021. The copyright holder for this preprint (which was not certified by peer review) is the author/funder, who has granted bioRxiv a license to display the preprint in perpetuity. It is made available under aCC-BY-NC 4.0 International license.

Anti-AtpΘ antiserum (rabbit antibodies)	Pineda Antibody-Service	this paper
Goat anti-rabbit secondary antibody	Sigma-Aldrich	Cat#A8275
Bacterial and virus strains		
Synechocystis sp. PCC 6803	Cyanolab	Strain PCC-M
Synechocystis sp. PCC 6803 (P_{atpT}-*atpT*)	This study	N/A
Synechocystis sp. PCC 6803 (P_{atpT}-*atpT*-3xFLAG)	This study	N/A
Synechocystis sp. PCC 6803 (AtpΘ-KO)	This study	N/A
Synechocystis sp. PCC 6803 (P_{petE}-sf*gfp*)	This study	N/A
Thermosynechococcus elongatus BP1	Gen Enomoto	N/A
Prochlorococcus sp. MED4	Claudia Steglich	N/A
Gloeobacter violaceus PCC 7421	Mai Watanabe	N/A
Nostoc sp. PCC 7120	Instituto de Bioquímica Vegetal y Fotosíntesis	N/A
Nostoc 7120 (GFP-less control)	This study	N/A
Nostoc 7120 (P_{atpT}-*gfp*)	This study	N/A
Nostoc 7120 (P_{atpT}-AtpΘ-GFP)	This study	N/A
Chemicals, peptides, and recombinant proteins		
Atpθ peptide	JPT Peptide Technologies GmbH	this paper
AcnSP peptide	JPT Peptide Technologies GmbH	de Alvarenga et al. (2020)[33]

bioRxiv preprint doi: https://doi.org/10.1101/2021.07.30.454416; this version posted October 15, 2021. The copyright holder for this preprint (which was not certified by peer review) is the author/funder, who has granted bioRxiv a license to display the preprint in perpetuity. It is made available under aCC-BY-NC 4.0 International license.

Atpθ_N peptide	JPT Peptide Technologies GmbH	this paper
Atpθ_C peptide	JPT Peptide Technologies GmbH	this paper
Atpθ_EE peptide	JPT Peptide Technologies GmbH	this paper
Atpθ_H peptide	JPT Peptide Technologies GmbH	this paper
Deposited data		
Mass spectrometry comparing co-immunoprecipitated proteins of Atpθ-3xFLAG and sfGFP-Atpθ (*n*=1)	ProteomeXchange	PXD020126
Mass spectrometry comparing co-immunoprecipitated proteins of Atpθ-3xFLAG and sfGFP-Atpθ (*n*=3; biological replicates)	ProteomeXchange	PXD024905
Oligonucleotides		
See **Table S3**		
Recombinant DNA		
See **Table S2**		
Software and algorithms		
Quantity One	Bio-Rad	Version 4.6.6
Confocal Software (LCS)	Leica	Version 2.61
GraphPad Prism	GraphPad Software, Inc.	Version 6.0

787

bioRxiv preprint doi: https://doi.org/10.1101/2021.07.30.454416; this version posted October 15, 2021. The copyright holder for this preprint (which was not certified by peer review) is the author/funder, who has granted bioRxiv a license to display the preprint in perpetuity. It is made available under aCC-BY-NC 4.0 International license.

Overview on Supplementary Tables

Table S1. Number of putative *atpT* homologs, lengths, isoelectric points and amino acid sequences of all predicted AtpΘ homologs in the listed cyanobacteria. An alternative start codon for the AtpΘ homolog in *Pseudanabaena* sp. PCC 7367 is marked in red.

Table S2. Plasmids and vectors used in this work.

Table S3. Primers and oligonucleotides used in this work. Nucleotides in boldface letters highlight the sequence of the T7 promoter.

Table S4. Mass spectrometry results of pull-down experiment. Subunits of the ATP synthase are marked in bold. “High” is written for the $\log_2$ fold change if the respective protein was not detected in either one or both of the controls (P_{atpT}-*atpT* and P_{petJ}-3xFLAG-*sfgfp*).

Table S5. Raw mass spectrometry results of the second pull-down experiment. The table lists all proteins identified together with their quantitative values. Proteins, which have not been identified in a given samples, are marked with n.d. (not detected). The normalized spectrum abundance factor (NSAF) is used for quantification. The higher abundant a protein is in the sample, the higher is its quantitative value. Protein abundance is also visualized by a color gradient from green (low abundance) over yellow to red (highly abundant).

Data S1. Details for the statistical analysis. (**A**) Details for the statistical analysis in **Figure 5A**. (**B**) Details for the statistical analysis in **Figure 5B**. (**C**) Details for the statistical analysis in **Figure 5C**. (**D**) Details for the statistical analysis in **Figure 5D**. (**E**) Details for the statistical analysis in **Figure 6D**. (**F**) Details for the statistical analysis in **Figure S3**.

bioRxiv preprint doi: https://doi.org/10.1101/2021.07.30.454416; this version posted October 15, 2021. The copyright holder for this preprint (which was not certified by peer review) is the author/funder, who has granted bioRxiv a license to display the preprint in perpetuity. It is made available under aCC-BY-NC 4.0 International license.

References

1. Kühlbrandt, W. (2019). Structure and mechanisms of F-type ATP synthases. Annu. Rev. Biochem. *88*, 515–549.
2. Gray, M.W. (2012). Mitochondrial evolution. Cold Spring Harb. Perspect. Biol. *4*, a011403.
3. Maréchal, E. (2018). Primary endosymbiosis: emergence of the primary chloroplast and the chromatophore, two independent events. Methods Mol. Biol. Clifton NJ *1829*, 3–16.
4. Martijn, J., Vosseberg, J., Guy, L., Offre, P., and Ettema, T.J.G. (2018). Deep mitochondrial origin outside the sampled alphaproteobacteria. Nature *557*, 101–105.
5. Mereschkowsky, C. (1905). Über natur und ursprung der chromatophoren im pflanzenreiche. Biol Cent. *25*, 593–604.
6. Ponce-Toledo, R.I., Deschamps, P., López-García, P., Zivanovic, Y., Benzerara, K., and Moreira, D. (2017). An early-branching freshwater cyanobacterium at the origin of plastids. Curr. Biol. *27*, 386–391.
7. Sagan, L. (1967). On the origin of mitosing cells. J. Theor. Biol. *14*, 255–274.
8. Hong, S., and Pedersen, P.L. (2008). ATP synthase and the actions of inhibitors utilized to study its roles in human health, disease, and other scientific areas. Microbiol. Mol. Biol. Rev. *72*, 590–641.
9. Pullman, M.E., and Monroy, G.C. (1963). A naturally occurring inhibitor of mitochondrial adenosine triphosphatase. J. Biol. Chem. *238*, 3762–3769.
10. Hashimoto, T., Yoshida, Y., and Tagawa, K. (1990). Regulatory proteins of F_1F_0-ATPase: role of ATPase inhibitor. J. Bioenerg. Biomembr. *22*, 27–38.
11. Hong, S., and Pedersen, P.L. (2002). ATP synthase of yeast: structural insight into the different inhibitory potencies of two regulatory peptides and identification of a new potential regulator. Arch. Biochem. Biophys. *405*, 38–43.
12. Solaini, G., Sgarbi, G., and Baracca, A. (2021). The F_1F_0-ATPase inhibitor, IF1, is a critical regulator of energy metabolism in cancer cells. Biochem. Soc. Trans., BST20200742.
13. Mendoza-Hoffmann, F., Pérez-Oseguera, Á., Cevallos, M.Á., Zarco-Zavala, M., Ortega, R., Peña-Segura, C., Espinoza-Simón, E., Uribe-Carvajal, S., and García-Trejo, J.J. (2018). The biological role of the ζ subunit as unidirectional inhibitor of the F_1F_0-ATPase of *Paracoccus denitrificans*. Cell Rep. *22*, 1067–1078.
14. Hahn, A., Vonck, J., Mills, D.J., Meier, T., and Kühlbrandt, W. (2018). Structure, mechanism, and regulation of the chloroplast ATP synthase. Science *360*, eaat4318.
15. Cozens, A.L., and Walker, J.E. (1987). The organization and sequence of the genes for ATP synthase subunits in the cyanobacterium *Synechococcus* 6301. Support for an endosymbiotic origin of chloroplasts. J. Mol. Biol. *194*, 359–383.
16. Nalin, C.M., and McCarty, R.E. (1984). Role of a disulfide bond in the gamma subunit in activation of the ATPase of chloroplast coupling factor 1. J. Biol. Chem. *259*, 7275–7280.
17. Miki, J., Maeda, M., Mukohata, Y., and Futai, M. (1988). The gamma-subunit of ATP synthase from spinach chloroplasts. Primary structure deduced from the cloned cDNA sequence. FEBS Lett. *232*, 221–226.
18. Mullineaux, C.W. (2014). Co-existence of photosynthetic and respiratory activities in cyanobacterial thylakoid membranes. Biochim. Biophys. Acta BBA - Bioenerg. *1837*, 503–511.

bioRxiv preprint doi: https://doi.org/10.1101/2021.07.30.454416; this version posted October 15, 2021. The copyright holder for this preprint (which was not certified by peer review) is the author/funder, who has granted bioRxiv a license to display the preprint in perpetuity. It is made available under aCC-BY-NC 4.0 International license.

19. Mullineaux, C.W., and Liu, L.-N. (2020). Membrane Dynamics in Phototrophic Bacteria. Annu. Rev. Microbiol. *74*, 633–654.
20. Sunamura, E.-I., Konno, H., Imashimizu-Kobayashi, M., Sugano, Y., and Hisabori, T. (2010). Physiological impact of intrinsic ADP inhibition of cyanobacterial F_0F_1 conferred by the inherent sequence inserted into the γ subunit. Plant Cell Physiol. *51*, 855–865.
21. Imashimizu, M., Bernát, G., Sunamura, E.-I., Broekmans, M., Konno, H., Isato, K., Rögner, M., and Hisabori, T. (2011). Regulation of F_0F_1-ATPase from *Synechocystis* sp. PCC 6803 by γ and ϵ subunits is significant for light/dark adaptation. J. Biol. Chem. *286*, 26595–26602.
22. Kopf, M., Klähn, S., Scholz, I., Matthiessen, J.K.F., Hess, W.R., and Voß, B. (2014). Comparative analysis of the primary transcriptome of *Synechocystis* sp. PCC 6803. DNA Res. *21*, 527–539.
23. Mitschke, J., Georg, J., Scholz, I., Sharma, C.M., Dienst, D., Bantscheff, J., Voß, B., Steglich, C., Wilde, A., Vogel, J., et al. (2011). An experimentally anchored map of transcriptional start sites in the model cyanobacterium *Synechocystis* sp. PCC6803. Proc. Natl. Acad. Sci. USA *108*, 2124–2129.
24. Baumgartner, D., Kopf, M., Klähn, S., Steglich, C., and Hess, W.R. (2016). Small proteins in cyanobacteria provide a paradigm for the functional analysis of the bacterial micro-proteome. BMC Microbiol. *16*, 285.
25. Mareš, J., Hrouzek, P., Kaňa, R., Ventura, S., Strunecký, O., and Komárek, J. (2013). The primitive thylakoid-less cyanobacterium *Gloeobacter* is a common rock-dwelling organism. PLOS ONE *8*, e66323.
26. Lou, P.-H., Hansen, B.S., Olsen, P.H., Tullin, S., Murphy, M.P., and Brand, M.D. (2007). Mitochondrial uncouplers with an extraordinary dynamic range. Biochem. J. *407*, 129–140.
27. Trebst, A. (2007). Inhibitors in the functional dissection of the photosynthetic electron transport system. Photosynth. Res. *92*, 217–224.
28. Rippka, R., Waterbury, J., and Cohen-Bazire, G. (1974). A cyanobacterium which lacks thylakoids. Arch. Microbiol. *100*, 419–436.
29. Partensky, F., Hess, W.R., and Vaulot, D. (1999). *Prochlorococcus*, a marine photosynthetic prokaryote of global significance. Microbiol. Mol. Biol. Rev. *63*, 106–127.
30. Mitschke, J., Vioque, A., Haas, F., Hess, W.R., and Muro-Pastor, A.M. (2011). Dynamics of transcriptional start site selection during nitrogen stress-induced cell differentiation in *Anabaena* sp. PCC 7120. Proc. Natl. Acad. Sci. USA *108*, 20130–20135.
31. Brenes-Álvarez, M., Olmedo-Verd, E., Vioque, A., and Muro-Pastor, A.M. (2016). Identification of conserved and potentially regulatory small RNAs in heterocystous cyanobacteria. Front. Microbiol. *7*, 48.
32. Washietl, S., Findeiss, S., Müller, S.A., Kalkhof, S., von Bergen, M., Hofacker, I.L., Stadler, P.F., and Goldman, N. (2011). RNAcode: robust discrimination of coding and noncoding regions in comparative sequence data. RNA *17*, 578–594.
33. de Alvarenga, L.V., Hess, W.R., Hagemann, M., and Hagemann, M. (2020). AcnSP - a novel small protein regulator of aconitase activity in the cyanobacterium *Synechocystis* sp. PCC 6803. Front. Microbiol. *11*, 1445.
34. Bulyha, I., Schmidt, C., Lenz, P., Jakovljevic, V., Höne, A., Maier, B., Hoppert, M., and Søgaard-Andersen, L. (2009). Regulation of the type IV pili molecular machine by dynamic localization of two motor proteins. Mol. Microbiol. *74*, 691–706.

bioRxiv preprint doi: https://doi.org/10.1101/2021.07.30.454416; this version posted October 15, 2021. The copyright holder for this preprint (which was not certified by peer review) is the author/funder, who has granted bioRxiv a license to display the preprint in perpetuity. It is made available under aCC-BY-NC 4.0 International license.

35. Okamoto, S., and Ohmori, M. (2002). The cyanobacterial PilT protein responsible for cell motility and transformation hydrolyzes ATP. Plant Cell Physiol. *43*, 1127–1136.
36. Lamiable, A., Thévenet, P., Rey, J., Vavrusa, M., Derreumaux, P., and Tufféry, P. (2016). PEP-FOLD3: faster de novo structure prediction for linear peptides in solution and in complex. Nucleic Acids Res. *44*, W449-454.
37. Gautier, R., Douguet, D., Antonny, B., and Drin, G. (2008). HELIQUEST: a web server to screen sequences with specific alpha-helical properties. Bioinforma. Oxf. Engl. *24*, 2101–2102.
38. Wu, Y., Li, Q., and Chen, X.-Z. (2007). Detecting protein-protein interactions by Far western blotting. Nat. Protoc. *2*, 3278–3284.
39. Sobti, M., Smits, C., Wong, A.S., Ishmukhametov, R., Stock, D., Sandin, S., and Stewart, A.G. (2016). Cryo-EM structures of the autoinhibited *E. coli* ATP synthase in three rotational states. eLife *5*, e21598.
40. Feniouk, B.A., Suzuki, T., and Yoshida, M. (2006). The role of subunit epsilon in the catalysis and regulation of F_0F_1-ATP synthase. Biochim. Biophys. Acta *1757*, 326–338.
41. Konno, H., Murakami-Fuse, T., Fujii, F., Koyama, F., Ueoka-Nakanishi, H., Pack, C.-G., Kinjo, M., and Hisabori, T. (2006). The regulator of the F_1 motor: inhibition of rotation of cyanobacterial F_1-ATPase by the epsilon subunit. EMBO J. *25*, 4596–4604.
42. Gu, J., Zhang, L., Zong, S., Guo, R., Liu, T., Yi, J., Wang, P., Zhuo, W., and Yang, M. (2019). Cryo-EM structure of the mammalian ATP synthase tetramer bound with inhibitory protein IF1. Science *364*, 1068–1075.
43. Quast, C., Pruesse, E., Yilmaz, P., Gerken, J., Schweer, T., Yarza, P., Peplies, J., and Glöckner, F.O. (2013). The SILVA ribosomal RNA gene database project: improved data processing and web-based tools. Nucleic Acids Res. *41*, D590-596.
44. Kumar, S., Stecher, G., Li, M., Knyaz, C., and Tamura, K. (2018). MEGA X: molecular evolutionary genetics analysis across computing platforms. Mol. Biol. Evol. *35*, 1547–1549.
45. Rzhetsky, A., and Nei, M. (1992). A simple method for estimating and testing minimum-evolution trees. Mol. Biol. Evol. *9*, 945–945.
46. Felsenstein, J. (1985). Confidence limits on phylogenies: an approach using the Bootstrap. Evolution *39*, 783–791.
47. Schägger, H. (2006). Tricine-SDS-PAGE. Nat. Protoc. *1*, 16–22.
48. Tusher, V.G., Tibshirani, R., and Chu, G. (2001). Significance analysis of microarrays applied to the ionizing radiation response. Proc. Natl. Acad. Sci. USA *98*, 5116–5121.
49. Lapashina, A.S., and Feniouk, B.A. (2018). ADP-inhibition of H^+-F_OF_1-ATP synthase. Biochem. Mosc. *83*, 1141–1160.
50. Rippka, R., Deruelles, J., Waterbury, J.B., Herdman, M., and Stanier, R.Y. (1979). Generic assignments, strain histories and properties of pure cultures of cyanobacteria. Microbiology *111*, 1–61.
51. Zhang, L., McSpadden, B., Pakrasi, H.B., and Whitmarsh, J. (1992). Copper-mediated regulation of cytochrome c553 and plastocyanin in the cyanobacterium *Synechocystis* 6803. J. Biol. Chem. *267*, 19054–19059.
52. Lippi, L., Bähr, L., Wüstenberg, A., Wilde, A., and Steuer, R. (2018). Exploring the potential of high-density cultivation of cyanobacteria for the production of cyanophycin. Algal Res. *31*, 363–366.

bioRxiv preprint doi: https://doi.org/10.1101/2021.07.30.454416; this version posted October 15, 2021. The copyright holder for this preprint (which was not certified by peer review) is the author/funder, who has granted bioRxiv a license to display the preprint in perpetuity. It is made available under aCC-BY-NC 4.0 International license.

53. Migur, A., Heyl, F., Fuss, J., Srikumar, A., Huettel, B., Steglich, C., Prakash, J.S.S., Reinhardt, R., Backofen, R., Owttrim, G.W., et al. (2021). The temperature-regulated DEAD-box RNA helicase CrhR interactome: Autoregulation and photosynthesis-related transcripts. J. Exp. Bot., erab416.
54. Allen, M.M. (1968). Simple conditions for growth of unicellular blue-green algae on plates. J. Phycol. *4*, 1–4.
55. Moore, L.R., Coe, A., Zinser, E.R., Saito, M.A., Sullivan, M.B., Lindell, D., Frois-Moniz, K., Waterbury, J., and Chisholm, S.W. (2007). Culturing the marine cyanobacterium *Prochlorococcus*. Limnol. Oceanogr. Methods *5*, 353–362.
56. Beyer, H.M., Gonschorek, P., Samodelov, S.L., Meier, M., Weber, W., and Zurbriggen, M.D. (2015). AQUA cloning: a versatile and simple enzyme-free cloning approach. PLOS ONE *10*, e0137652.
57. Olmedo-Verd, E., Muro-Pastor, A.M., Flores, E., and Herrero, A. (2006). Localized induction of the *ntcA* regulatory gene in developing heterocysts of *Anabaena* sp. strain PCC 7120. J. Bacteriol. *188*, 6694–6699.
58. Brenes-Álvarez, M., Mitschke, J., Olmedo-Verd, E., Georg, J., Hess, W.R., Vioque, A., and Muro-Pastor, A.M. (2019). Elements of the heterocyst-specific transcriptome unravelled by co-expression analysis in *Nostoc* sp. PCC 7120. Environ. Microbiol. *21*, 2544–2558.
59. Muro-Pastor, A.M., Flores, E., and Herrero, A. (2009). NtcA-regulated heterocyst differentiation genes *hetC* and *devB* from *Anabaena* sp. strain PCC 7120 exhibit a similar tandem promoter arrangement. J. Bacteriol. *191*, 5765–5774.
60. Markowitz, V.M., Chen, I.-M.A., Palaniappan, K., Chu, K., Szeto, E., Grechkin, Y., Ratner, A., Jacob, B., Huang, J., Williams, P., et al. (2012). IMG: the Integrated Microbial Genomes database and comparative analysis system. Nucleic Acids Res. *40*, D115-122.
61. Gertz, E.M., Yu, Y.-K., Agarwala, R., Schäffer, A.A., and Altschul, S.F. (2006). Composition-based statistics and translated nucleotide searches: Improving the TBLASTN module of BLAST. BMC Biol. *4*, 41.
62. Altschul, S.F. (2014). BLAST Algorithm. In eLS (American Cancer Society).
63. Waterhouse, A.M., Procter, J.B., Martin, D.M.A., Clamp, M., and Barton, G.J. (2009). Jalview Version 2—a multiple sequence alignment editor and analysis workbench. Bioinformatics *25*, 1189–1191.
64. Audain, E., Ramos, Y., Hermjakob, H., Flower, D.R., and Perez-Riverol, Y. (2016). Accurate estimation of isoelectric point of protein and peptide based on amino acid sequences. Bioinforma. Oxf. Engl. *32*, 821–827.
65. Klähn, S., Baumgartner, D., Pfreundt, U., Voigt, K., Schön, V., Steglich, C., and Hess, W.R. (2014). Alkane biosynthesis genes in cyanobacteria and their transcriptional organization. Front. Bioeng. Biotechnol. *2*, 24.
66. Tamura, K., Nei, M., and Kumar, S. (2004). Prospects for inferring very large phylogenies by using the neighbor-joining method. Proc. Natl. Acad. Sci. USA *101*, 11030–11035.
67. Muro-Pastor, A.M. (2014). The heterocyst-specific NsiR1 small RNA is an early marker of cell differentiation in cyanobacterial filaments. mBio *5*, e01079-01014.
68. Bonn, F., Bartel, J., Büttner, K., Hecker, M., Otto, A., and Becher, D. (2014). Picking vanished proteins from the void: how to collect and ship/share extremely dilute proteins in a reproducible and highly efficient manner. Anal. Chem. *86*, 7421–7427.
69. Tyanova, S., Temu, T., Sinitcyn, P., Carlson, A., Hein, M.Y., Geiger, T., Mann, M., and Cox, J. (2016). The Perseus computational platform for comprehensive analysis of (prote)omics data. Nat. Methods *13*, 731–740.

bioRxiv preprint doi: https://doi.org/10.1101/2021.07.30.454416; this version posted October 15, 2021. The copyright holder for this preprint (which was not certified by peer review) is the author/funder, who has granted bioRxiv a license to display the preprint in perpetuity. It is made available under aCC-BY-NC 4.0 International license.

70. Pinto, F.L., Thapper, A., Sontheim, W., and Lindblad, P. (2009). Analysis of current and alternative phenol based RNA extraction methodologies for cyanobacteria. BMC Mol. Biol. *10*, 79.
71. Mohamed, A., and Jansson, C. (1989). Influence of light on accumulation of photosynthesis-specific transcripts in the cyanobacterium *Synechocystis* 6803. Plant Mol. Biol. *13*, 693–700.
72. Dong, Y., and Xu, X. (2009). Outer membrane proteins induced by iron deficiency in *Anabaena* sp. PCC 7120. Prog. Nat. Sci. *19*, 1477–1483.
73. Krauspe, V., Fahrner, M., Spät, P., Steglich, C., Frankenberg-Dinkel, N., Maček, B., Schilling, O., and Hess, W.R. (2021). Discovery of a novel small protein factor involved in the coordinated degradation of phycobilisomes in cyanobacteria. Proc. Natl. Acad. Sci. USA *118*, e2012277118.